EDESR and ODMR Spectroscopy of Point Defects in SemiconductorNanostructures

Nikolai T. Bagraev[1], Ekaterina N. Kalabukhova[2], Vyacheslav S. Khromov[1], Leonid E. Klyachkin[1], Anna M. Malyarenko[1],Dariya V. Savchenko[2, 3], Bela D. Shanina[2]
[1]Ioffe Institute, 194021, St.Petersburg, Russia
[2]Lashkaryov Institute of Semiconductor Physics, NASU, Kyiv, Ukraine
[3]Institute of Physics, AS CR, Praha, Czech Republica

Abstract: We present the first findings of the new electrically- and optically-detected magnetic resonance technique (EDESR and ODMR) which reveal single point defects in the ultra-narrow silicon quantum wells (Si-QW) confined by the superconductor δ-barriers. This technique allows the ESR identification without the application of the external cavity as well as the hf source and recorder, with measuring the only magnetoresistance (EDESR) and transmission (ODMR) spectra within frameworks of the excitonic normal-mode coupling (NMC) caused by the microcavities embedded in the Si-QW plane. The new resonant positive magnetoresistance data are interpreted here in terms of the interference transition in the diffusive transport of free holes respectively between the weak anti-localization regime in the region far from the ESR of a paramagnetic point defect located inside or near the conductive channel and the weak localization regime in the nearest region of the ESR of that defect. The new EDESR technique as well as the standard ESR technique is applied also for the studies of the silicon vacancy related centers identified in the non-irradiated 6H-SiC nanostructure. This planar 6H-SiC nanostructure represents the ultra-narrow p-type quantum well confined by the δ-barriers heavily doped with boron on the surface of the n-type 6H-SiC (0001) wafer. The new EDESR technique by measuring the only magnetoresistance of the 6H-SiC nanostructure under the high frequency generation from the δ-barriers appears to allow the identification of the isolated silicon vacancy centers as well as the triplet center with spin state S=1. The same triplet center that is characterized by the large value of the zero-field splitting constant D and anisotropic g-factor is revealed by the ESR (X-band) method. The hyperfine (HF) lines in the ESR and EDESR spectra originating from the HF interaction with the 14N nucleus seem to attribute this triplet center to the N-VSi defect.

Keywords: EDESR and ODMR technique, ultra-narrow silicon quantum wells, superconductor δ-barriers, 6H-SiC nanostructure, weak localization.

I. INTRODUCTION

Spin-dependent transport through semiconductor nanostructures inserted in nano- and microcavities between superconductor leads is of great interest to identify the magnetic resonance phenomena without using both the external cavity and the external hf sources and recorders [1, 2]. One of the best candidate for the role of such a ‘sandwich’ structure that is able to demonstrate the electrically- and optically-detected ESR (EDESR and ODMR) appears to be the high mobility p-type silicon quantum well (Si-QW), 2nm, confined by the δ-barriers heavily doped with boron on the n-type Si (100) surface (Figs. 1 and 2). The boron centers inside the δ-barriers are found to be the impurity dipoles, B^+-B^-, which are a basis of their high temperature superconductor (HTS) properties, if the sheet density of the 2D holes in the Si-QW becomes to be more than 10^{11} cm^{-2} (Figs. 3 a and b) [2, 3]. The findings of the electrical resistivity, thermo-emf, specific heat and magnetic susceptibility measurements are actually

evidence of the superconductor properties for these •-barriers, 3 nm, N(B)=5 10^{21} cm^{-3} [3]. These silicon nanostructures embedded in superconductor shells have been shown to be the type II high temperature superconductors (HTS) with T_c=145 K and H_{c2}=0.22 T [2]. The superconductor gap appeared to result in the THz and GHz generation under applied voltage [2, 3]. Spectroscopic studies confirmed this pattern and furthermore showed that the hf emission can be enhanced, if the Si-QW is incorporated into the fractal silicon microcavity system [1]. The goal of the present work is to study the EDESR and the ODMR of single point defects inserted into the Si-QW in the absence of the external cavity resonator as well as the hf source and recorder by measuring the only magnetoresistance (EDESR) and transmission (ODMR) spectra within frameworks of the excitonic normal-mode coupling (NMC) with a single Si-QW inside a 1λ silicon microcavity. This excitonic NMC regime appears to favour the giant triplet-singlet splitting caused by the exchange interaction of the impurity electron states with the s-p electronic states of the host Si-QW which is revealed by the transmission spectra under the formation of the bound exciton at an impurity center [4, 5].

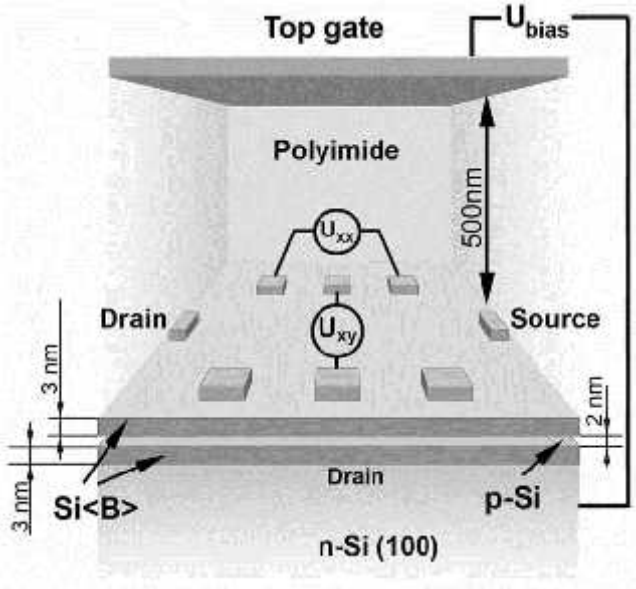

Fig. 1. The schematic diagram of the experimental device that demonstrates a perspective view of the p-type Si-QW confined by the δ-barriers heavily doped with boron on the n-type Si (100) surface. The top gate is able to control the sheet density of holes and the Rashba SOI value. The depletion regions indicate the Hall geometry of leads.

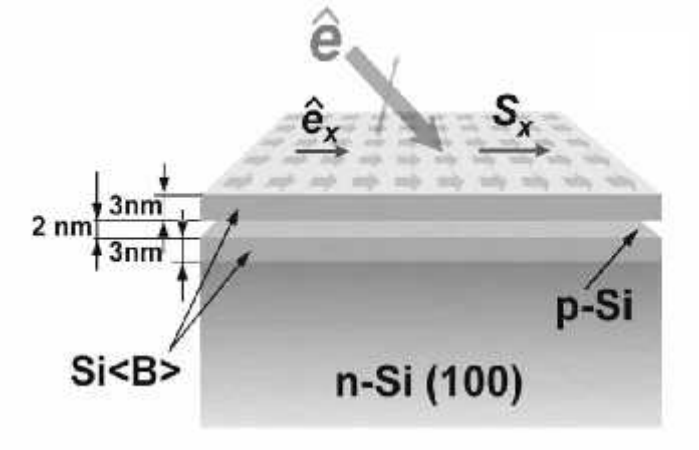

Fig. 2. The ODMR transmission experiment with the p-type silicon quantum well confined by the δ-barriers containing the dipole centers of boron, which is prepared on the n-type Si (100) surface. The effective exchange field is caused by forming the bound excitons under the optical illumination with linearly polarized light.

Recently the N-V_{Si}- (S=1) defect in the diamond, silicon carbide 4H-and 6H-SiC structures became to be of interest as a qubit for quantum computing operations owing to the possibility to control the coherent spin processes at room temperature [6-10]. However, up to now the N-V_{Si} defect and other

silicon vacancy related centers were introduced into these wide gap semiconductors only by the neutron, proton and electron irradiation with subsequent thermal annealing. Therefore the preparation of samples containing the only N-V_{Si} defects and isolated silicon vacancies for the realization of the qubit versions has been always difficult because of the different defects created under this irradiation which are able to give rise to the non-radiative recombination. In present work we demonstrate also the results of the ESR and EDESR studies of the N-V_{Si} defect and the isolated silicon vacancy centers which are formed in the course of the preparation of the planar 6H-SiC nanostructure without any previous or subsequent e- and n- irradiation. The new EDESR technique used here allows the identification of point and extended defects by measuring the only magnetoresistance without application of an external cavity as well as a hf source and recorder, with internal high frequency generation within frameworks of the normal-mode coupling (NMC) caused by the microcavities embedded in a semiconductor nanostructure [11].

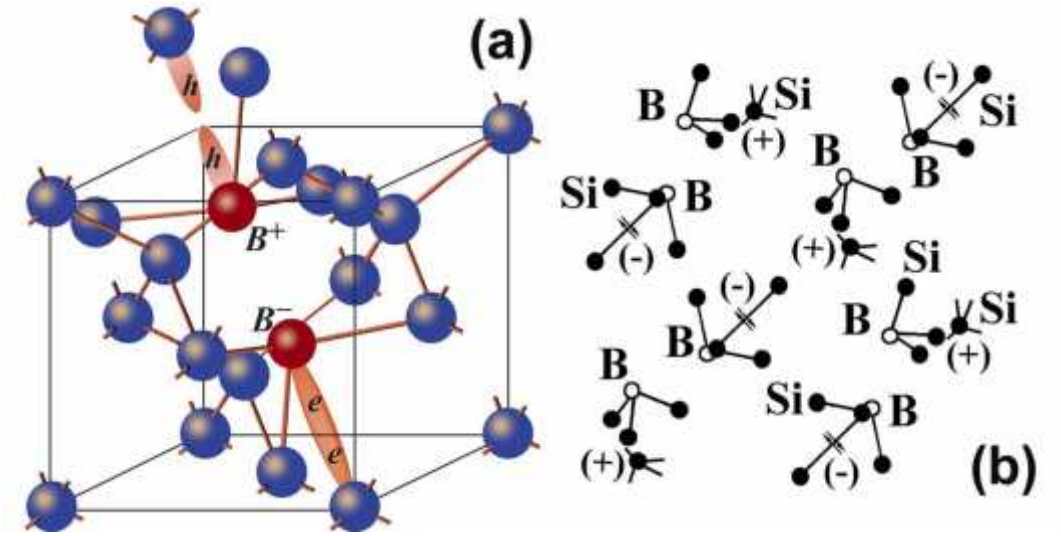

Fig. 3. (a) Model for the elastic reconstruction of a shallow boron acceptor, which is accompanied by the formation of the trigonal dipole (B^+ - B^-) centers as a result of the negative-U reaction: $2B^o \rightarrow B^+ + B^-$. (b) A series of the dipole negative-U centers of boron located between the undoped microdefects that seem to be a basis of nanostructured δ - barriers confining the Si-QW.

II. METHODS

The energy positions of the two-dimensional subbands of holes in the Si-QW and the value of the superconductor gap, 2Δ=0.044 eV, caused by the superconductor δ-barriers were determined in the studies of the far-infrared and tunneling spectroscopy (Figs. 4 a, b, c and d) [2, 3]. The results obtained are in a good agreement with corresponding calculations following by Ref [12] if the width of the Si-QW, 2nm, is taken into account (Fig. 4 b).

The Si-QWs confined by the δ-barriers heavily doped with boron on the n-type Si (100) surface were also identified by the four-point probe method using layer-by-layer etching and by the cyclotron resonance (CR) angular dependencies [13]. These CR measurements were performed at 3.8 K with a standard Brucker-Physik AG ESR spectrometer at X-band (9.1-9.5 GHz). The rotation of the magnetic field in a plane normal to the diffusion profile plane has revealed the anisotropy of both the electron and hole effective masses in silicon bulk and the Landau levels scheme in Si-QWs. This CR quenching and the line shifts for which a characteristic 180^o symmetry was observed can be explained with the effect of the electrical field created by the confining potential inside p^+-diffusion profile and its

different arrangement in the longitudinal and lateral Si-QWs formed naturally between the δ-barriers heavily doped with boron [13]. The observed different behavior of the heavy and light holes may be explained by lifting the degeneracy between the $J_z = \pm 3/2$ and $J_z = \pm 1/2$ valence bands for $k = 0$ due to the confining potential.

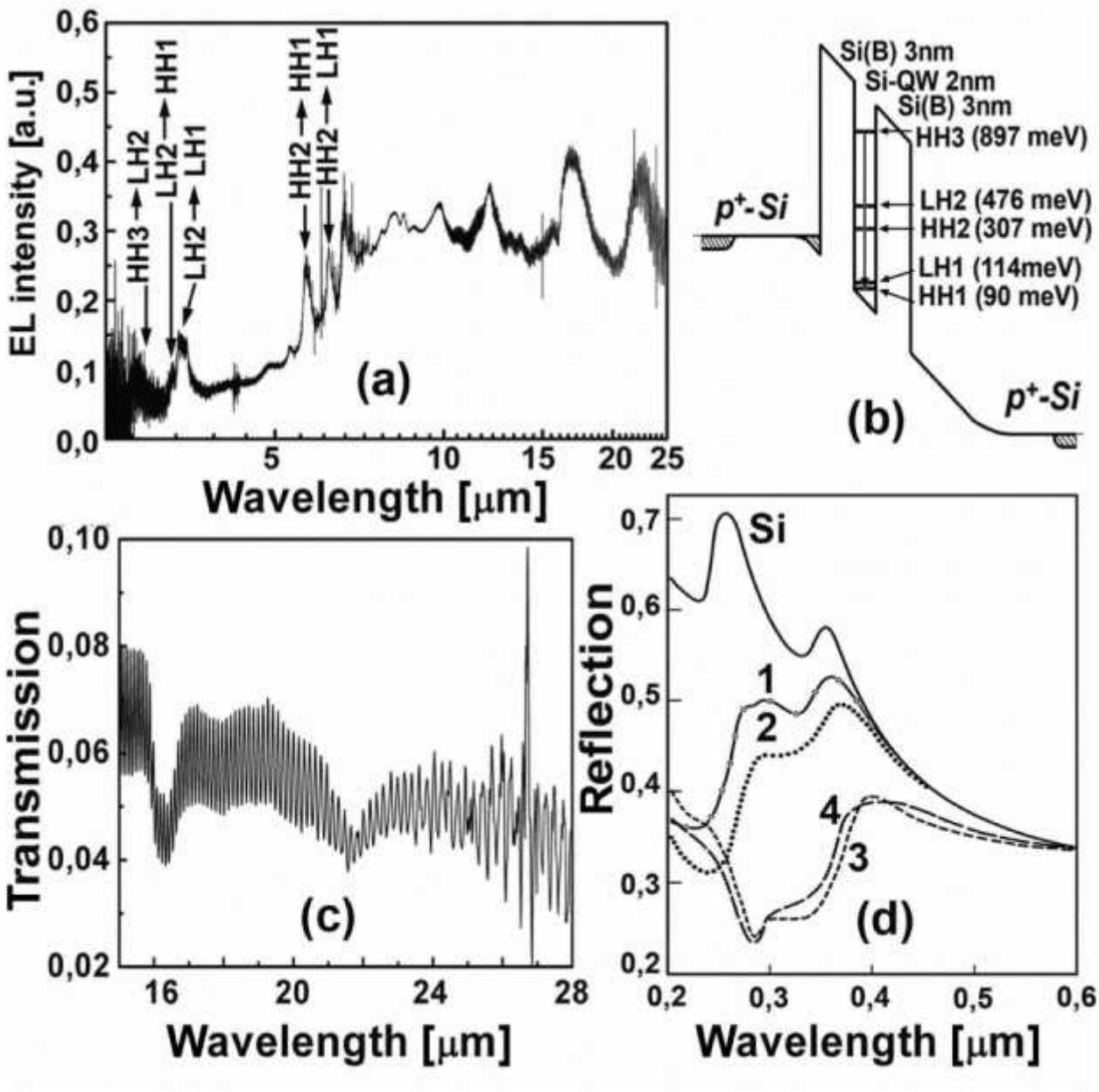

Fig. 4. Electroluminescence spectrum (a) that defines the energies of two-dimensional subbands of heavy and light holes in the p-type Si-QW confined by the δ - barriers heavily doped with boron on the n-type Si (100) surface (b). (c) Transmission spectrum that reveals both the local phonon mode, λ = 16.4 μm, and the superconductor gap, λ = 26.9 μm, manifestation. (d) The reflection spectra from the n - type Si (100) surface and from the ultra-shallow boron diffusion profiles prepared on the n - type Si (100) surface that consist of the δ barriers confining the ultra-narrow Si-QW. The curves 1-4 are related to the δ barriers with different concentration of boron. The values of the concentration boron in different samples are characterized by the following ratio: curve 1 – 0.2, 2 – 0.3, 3 – 0.35, 4 -0.4. The concentration of boron in the sample characterized by the fourth curve is equal to $5 \cdot 10^{21}$ cm^{-3}.

The STM technique was used to control the formation of the fractal distribution of the self-interstitials microdefects inside the δ barriers that confine the Si-QW (Figs. 5 a, b and c). The STM images demonstrate that the ratio between the dimensions of the microdefects that are displayed as light poles in Figs. 5 a and c is supported to be equal to 3.3 thereby defining the self-assembly of the self-interstitials microdefects as the self-organization of the fractal type (Fig. 5 b). The analysis of the STM image in detail has shown that the dimension of the smallest microdefect observed in fractal series, ~2nm, is consistent with the parameters expected from the tetrahedral model of the Si60 cluster (Fig. 5 c) [14].

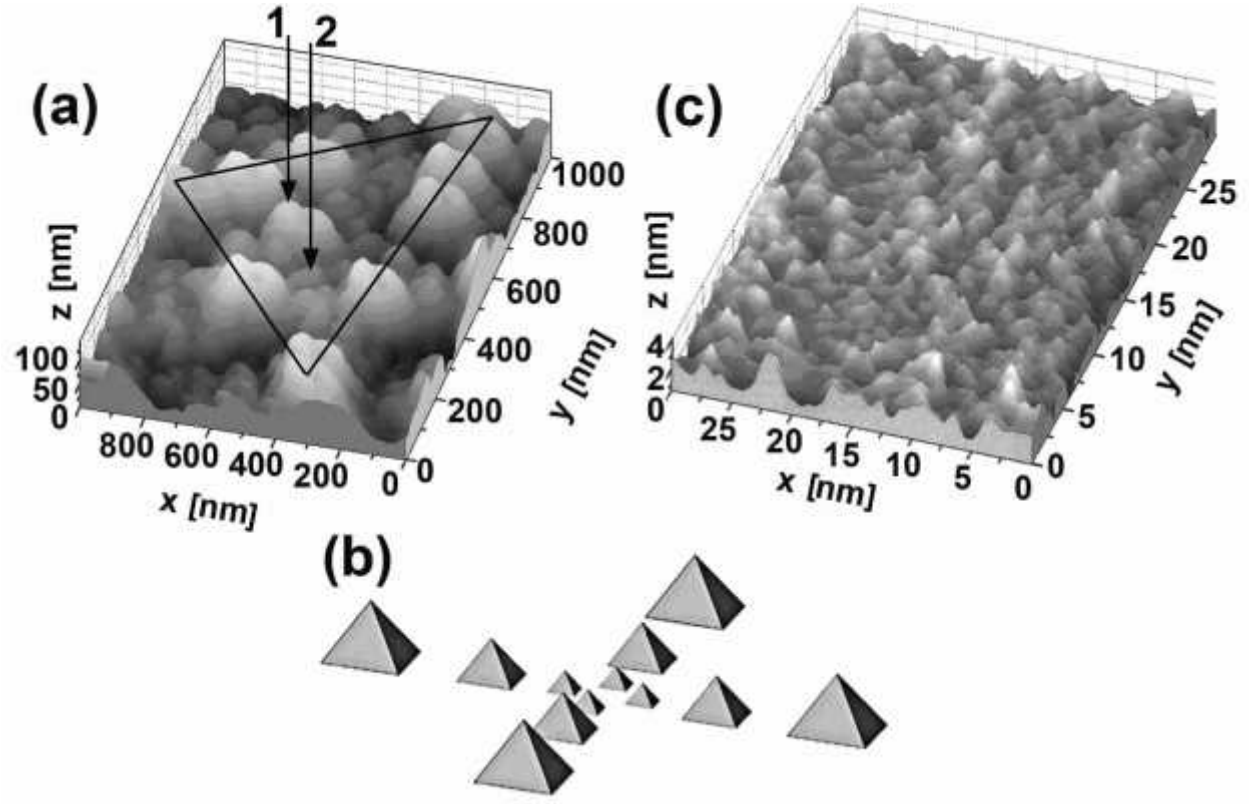

Fig. 5. (a) - STM image of the ultra-shallow boron diffusion profile prepared at the diffusion temperature of 800°C into the Si(100) wafer covered previously by medium oxide overlayer X||[001], Y||[010], Z||[100]. Solid triangle and arrows that are labeled as 1 and 2 exhibit the microdefects with dimensions 740 nm, 225 nm and 68 nm, respectively, which are evidence of their fractal self-assembly.
(b) - The model of the self-assembled microcavity system formed by the microdefects of the fractal type on the Si (100) surface.
(c) - STM image of the ultra-shallow boron diffusion profile prepared at diffusion temperature of 900°C into the Si (100) wafer covered previously by medium oxide overlayer. X||[001], Y||[010], Z||[100].

Thus, the δ - barriers, 3 nm, heavily doped with boron, 5 10^{21} cm^{-3}, represent really alternating arrays of the smallest undoped microdefects and doped dots with dimensions restricted to 2 nm (Fig. 5 c). The value of the boron concentration determined by the SIMS method seems to indicate that each doped dot located between undoped microdefects contains two impurity atoms of boron. Since the boron dopants form shallow acceptor centers in the silicon lattice, such high concentration has to cause a metallic-like conductivity. Nevertheless, the angular dependencies of the cyclotron resonance spectra demonstrate

that the p-type Si-QW confined by the δ - barriers heavily doped with boron contains the high mobility 2D hole gas which is characterized by long momentum relaxation time of the heavy and light holes at 3.8 K, $\tau \geq 5 \cdot 10^{-10}$ s [13, 15]. Thus, the momentum relaxation time of holes in the ultra-narrow Si-QW appeared to be longer than in the best MOS structures contrary to what might be expected from strong scattering by the heavily doped δ - barriers. This passive role of the δ - barriers between which the Si-QW is formed was quite surprising, when one takes into account the high level of their boron doping. To eliminate this contradiction, the ESR technique has been applied for the studies of the boron centers packed up in dots [15, 16]. The angular dependences of the ESR spectra at different temperatures in the 3.8÷27 K range that reveal the trigonal symmetry of the boron dipole centers have been obtained with the same ESR spectrometer, the Brucker-Physik AG ESR spectrometer at X-band (9.1-9.5 GHz), with the rotation of the magnetic field in the {110}-plane perpendicular to a {100}-interface (B_{ext} = 0°, 180° parallel to the Si-QW plane, Bext = 90° perpendicular to the Si-QW plane) (Figs. 6 a, b, c and d). No ESR signals in the X-band are observed, if the Si-QW confined by the δ - barriers is cooled down in the external magnetic field (B_{ext}) weaker than 0.22 T, with the persistence of the amplitude and the resonance field of the trigonal ESR spectrum as function of the crystallographic orientation and the magnetic field value during cooling down process at $B_{ext} \geq 0.22$ T (Figs. 6 a, b and c). With increasing temperature, the ESR line observed changes its magnetic resonance field position and disappears at 27 K (Fig. 6 c).

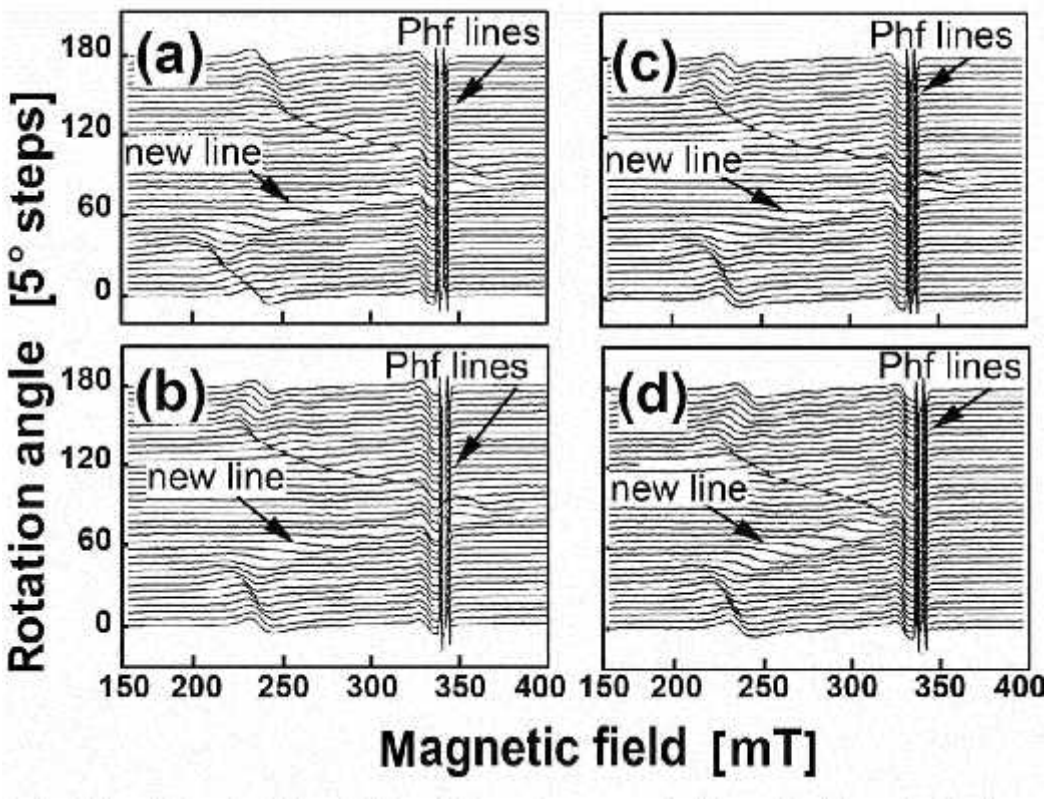

Fig. 6. The trigonal ESR spectrum observed in field cooled ultra-shallow boron diffusion profile that seems to be evidence of the dynamic magnetic moment due to the trigonal dipole centers of boron inside the δ - barriers confining the Si-QW which is persisted by varying both the temperature and magnetic field values. B_{ext} || <110> (a), || <112> (b), || <111> (c, d). Rotation of the magnetic field in the {110}-plane perpendicular to a {100}-interface ($B_{ext} = 0^o$, 180^o || interface, $B_{ext} = 90^o \perp$ interface), ν = 9.45 GHz, T = 14 K (a, b, c) and T=21 K (d).

The observation of the ESR spectrum is evidence of the fall in the electrical activity of shallow boron acceptors contrary to high level of boron doping. Therefore, the trigonal ESR spectrum observed seems to be evidence of the dynamic magnetic moment that is induced by the exchange interaction between the small hole bipolarons which are formed by the negative-U reconstruction of the shallow boron acceptors, $2B0 \rightarrow B^+ + B^-$, along the <111> crystallographic axis (Fig. 3 a) [13, 16, 17]. These small hole bipolarons localized at the dipole boron centers, $B^+ - B^-$, seem to undergo the singlet-triplet transition in the process of the exchange interaction through the holes in the Si-QW thereby leading to the trigonal ESR spectrum (Figs. 6 a, b, c and d). Besides, the sublattice of the hole bipolarons located between the undoped microdefects appears to define the one-electron band scheme of the δ - barriers as well as the transport properties for the 2D gas of holes in the Si-QW (Figs. 4 b and 4 d) [16].

In order to determine the one-electron band scheme of the δ - barriers that confine the Si-QW, the reflection spectra R(λ) were studied using a UV-VIS Specord M-40 spectrophotometer with an Ulbricht sphere for the reflectivity measurements [18]. Fig. 4 d shows the spectra of the reflection from the δ - barriers with different concentration of boron. The decrease in R(λ) compared with the data of the silicon single crystal and the drops in the position of the peaks at the wavelengths of λ=354 and 275 nm are observed. The above peaks are related to the transitions between Γ-L valleys and in the vicinity of the point X in the Brillouin zone, with the former of the above peaks being assigned to the direct transition $\Gamma'_{25} - \Gamma'_2$, whereas the latter peak is attributed to the transition $X_4 - X_1$. An analysis of the spectral dependence of the reflection coefficient shows that the presence of the microcavities formed by the self-assembled microdefects with medium size reduces R(λ) most profoundly in the short-wavelength region of the spectrum (200-300 nm). It follows from the comparison of R(λ) with the STM data that the position of the minima in the reflection coefficient in the spectral dependence R(λ) and the microcavity size are interrelated and satisfy the Bragg condition, $x = \lambda/2n$, where x is the cavity size, λ is the wavelength, and n is the refractive index of silicon, n=3.4. The R(λ) drop in the position of the $\Gamma'_{25} - \Gamma'_2$ and $X_4 - X_1$ transitions appears to be due to the formation of the wide-gap semiconductor layer with increasing the concentration of boron. These data substantiate the assumption noticed above that the role of the dot containing the small hole bipolaron is to establish the band structure of the δ - barrier with the energy confinement more than 1.25eV in both the conduction and the valence band of the Si-QW (Fig. 4 d).

In order to identify the transfer of the small hole bipolarons as a possible mechanism of superconductivity, the transport of holes in the S-Si-QW-S structures is followed to be studied at different orientation of the external magnetic field relatively to the Si-QW plane. The dependences of the longitudinal voltage on the magnetic field value shown in Fig. 7 are evidence of the Zeeman effect that seems to be due to the creation of the triplet and singlet states of the small hole bipolarons localized at the dipole boron centers (Fig. 3 a). The sign inversion of the U_{xx} voltage is of importance to result from the change of the magnetic field direction to opposite. Thus, the transport of the small hole bipolarons that can be captured and/or scattered on the dipole boron centers seems to be caused by the diamagnetic response induced by applying a magnetic field. Besides, the magnetic field dependences of the U_{xx} voltage considered within frameworks of the triplet, T^+, T^0, T^-, as well as the ground, S_0^+, S_0^-, and excited, S_1^+, S_1^-, states undergone by the Zeeman splitting appear to reveal the presence of the upper critical magnetic field H_{c2} and the oscillations of the critical current which are in a good agreement with the measurements of the ESR spectra (Figs. 6 a-c) and the field and temperature magnetic susceptibility dependencies [2]. The resonance behaviour of the $U_{xx}(H)$ dependences in the anti-crossing points of the triplet sublevels (T^+-T^0) is evidence of the spin polarization that results from the selective population or depopulation of the T^+ and T^- states relatively to the T^0 state in consequence of the partial removal of a ban on the forbidden triplet-singlet transitions [19]. The spin polarization of

the bipolarons in the triplet state in the S-Si-QW-S structures should be of importance in the studies of the spin interference caused by the Rashba spin-orbit interaction in the quantum wires and rings [20, 21]. The creation of the excited singlet states in the processes of the bipolaronic transport is also bound to be noticed, because owing to the transitions from the excited to the ground singlet state of the small hole bipolarons these 'sandwich' structures seem to be perspective as the sources and recorders of the THz and GHz emission that is revealed specifically in the electroluminescence spectra as a low frequency modulation (see Fig. 4 a). Here these effects will be present as the EDESR and ODMR spectra of the single impurity centers in the Si-QW confined by the δ-barriers heavily doped with boron which are especially performed by the direct measurements of the magnetic resistance and transmission spectra under such an internal THz and GHz emission in the absence of the external cavity resonator [1, 22]. The extremely low value of the effective mass of the 2D holes in the 'sandwich' S-Si-QW-S structures that results from the CR measurements and the studies of the Aharonov-Casher oscillations [3] seems to be the principal argument for the bipolaronic mechanism of high temperature superconductor properties which is based on the coherent tunneling of bipolarons [23, 24].

The local phonon mode manifestation at $\lambda = 16.4$ μm that presents, among the superconductor gap, $\lambda = 26.9$ μm <=> 2Δ, in the transmission spectrum favours the use of this conception (Fig. 4 c). High frequency local phonon mode, $\lambda = 16.4$ μm <=> 76 meV, appears to exist simultaneously with the intermediate value of the coupling constant, κ. The value of the coupling constant, $\kappa = VN(0)$, is derived from the BCS formula $\Delta = 2\hbar\omega_D \exp(-1/\kappa)$ taking account of the experimental values of the superconductor energy gap, $2\Delta = 0.044$ eV, and the local phonon mode energy, $\hbar\omega_D = 76$ meV. This estimation results in $\kappa \approx 0.52$ that is outside the range 0.1÷0.3 for metallic low-temperature superconductors with weak coupling described within the BCS approach. Therefore the superconductor properties of the 'sandwich' S-Si-QW-S structures seem to be due to the transfer of the mobile small hole bipolarons that gives rise to the high T_c value owing to small effective mass.

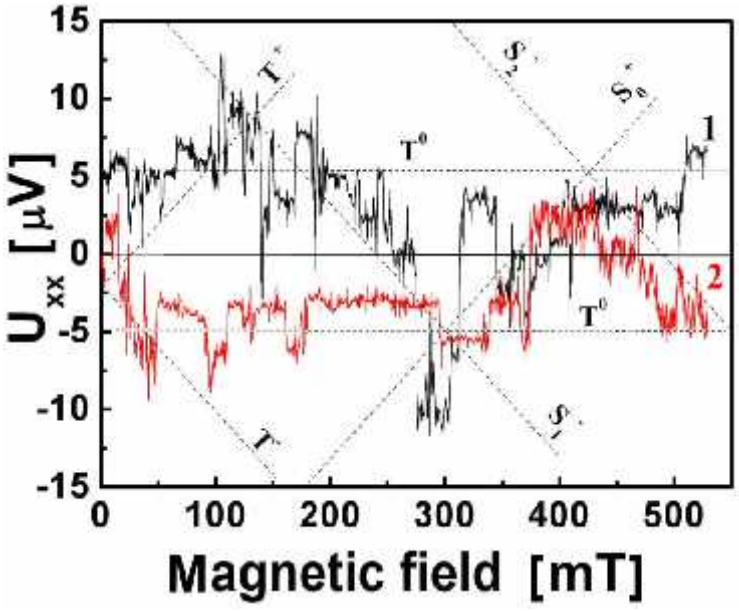

Fig. 7. U_{xx} vs the value of the magnetic field applied perpendicularly to the plane of the p-type Si-QW confined by the δ-barriers on the n-type Si (100) surface. I_{ds}=10 nA. T=77 K. Curves 1 and 2 measured for opposite orientations of a magnetic field reveal the sign of U_{xx} that corresponds to the diamagnetic response of the superconductor δ-barriers.

The results obtained have a bearing on the versions of the high temperature superconductivity that are based on the promising application of the sandwiches which consist of the alternating superconductor and insulator layers [25-28]. In the latter case, a series of heavily doped with boron and undoped silicon dots that forms the Josephson junction area in nanostructured δ - barriers is of

advantage to achieve the high T_c value, $T_c = (\hbar\omega_D/k_B)\exp(-N(0)V)$, because of the presence of the local high frequency phonon mode which compensates for the relatively low density of states, N(0). Nevertheless, the mechanism of the bipolaronic transfer is still far from completely clear. This raises the question of whether the Josephson transitions dominate in the transfer of the pair of 2D holes in the plane of the nanostructured δ - barriers and in the proximity effect due to the tunneling through the Si-QW or the Andreev reflection plays a part in the bipolaronic transfer similar to the successive two-electron (hole) capture at the negative-U centers [29, 30]. The superconductor gap, $2\Delta = 0.044$ eV, appeared to be the source of the THz emission due to the Josephson junctions self-assembled in the sandwich structure (Figs. 1 and 2). Moreover, since the high temperature superconductor properties for the δ-barriers result from the transfer of the small hole bipolarons through these negative-U dipole centers of boron, this transport of 2D holes is able to cause the GHz generation under applied voltage, optical pumping or by scanning external magnetic field with the enhancement by varying the positions of the leads within frameworks of the Hall geometry (Figs. 1 and 2) [1, 4, 5]. Spectroscopic studies of the Rabi splitting in the THz and GHz ranges have confirmed the described pattern and furthermore demonstrated that the area of the δ-barrier defines the dimensions of the THz and GHz cavities incorporated into the Si-QW. Thus, the sandwich structure provides the THZ and GHz generation thereby giving rise to the EDESR and ODMR measurements of single impurity centers without using the external cavity as well as the hf source and recorder.

Finally, the THz and GHz emission from the δ-barriers that is a basis of the new technique suggested was additionally controlled by measuring of the Shapiro steps [31]. This type of steps in the CV characteristics of the Josephson junctions is caused by the external hf illumination, with the voltage step equal to $\Delta U = h\nu/2e$; here ν is frequency of the hf illumination. Therefore, we have used the experimental device studied as a hf recorder, whereas the device structure with identical parameters was applied to be a hf source (Fig. 8). The level of the drain-source current in both device structures was stabilized at the value of 10 nA. The intricate behavior of the steps in the Josephson CV characteristics is revealed by stepwise varying, see Figs. 9 a and b, 10. Using the relationship, $\Delta U = h\nu/2e$, we appear to define the frequencies of the Josephson generation equal respectively to 9.1 GHz and 120 GHz (Figs. 9 a and b) as well as 5.3 THz and 10.6 THz (Fig. 10). This observation became it possible, because the special microcavities have been incorporated into the Si-QW plane, with the sizes corresponding to the frequencies noticed above, $L=\lambda/2n$; here n is the refractive index, $n=3.4$, L is the microcavity size and λ is the wavelength of the GHz-radiation.

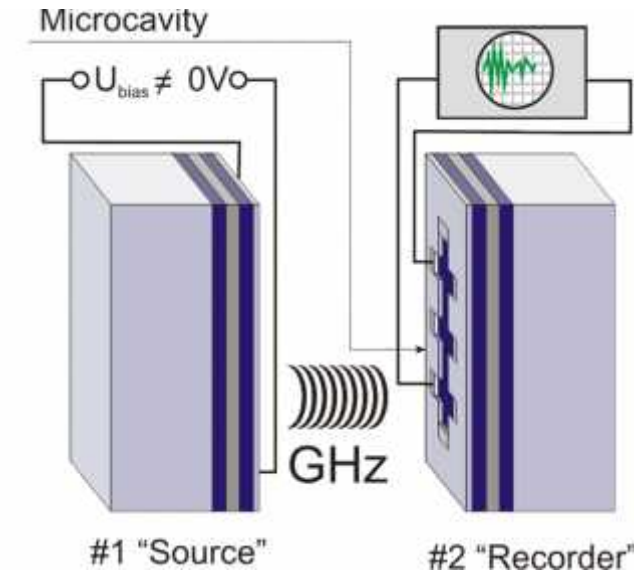

Fig. 8. The Shapiro steps experiment. Two identical experimental devices shown in Fig. 1 are used as a hf recorder and a hf source to observe the Shapiro steps caused by the hf illumination in the Josephson CV characteristic. The level of the drain-source current in both device structures was stabilized at the value of 10 nA.

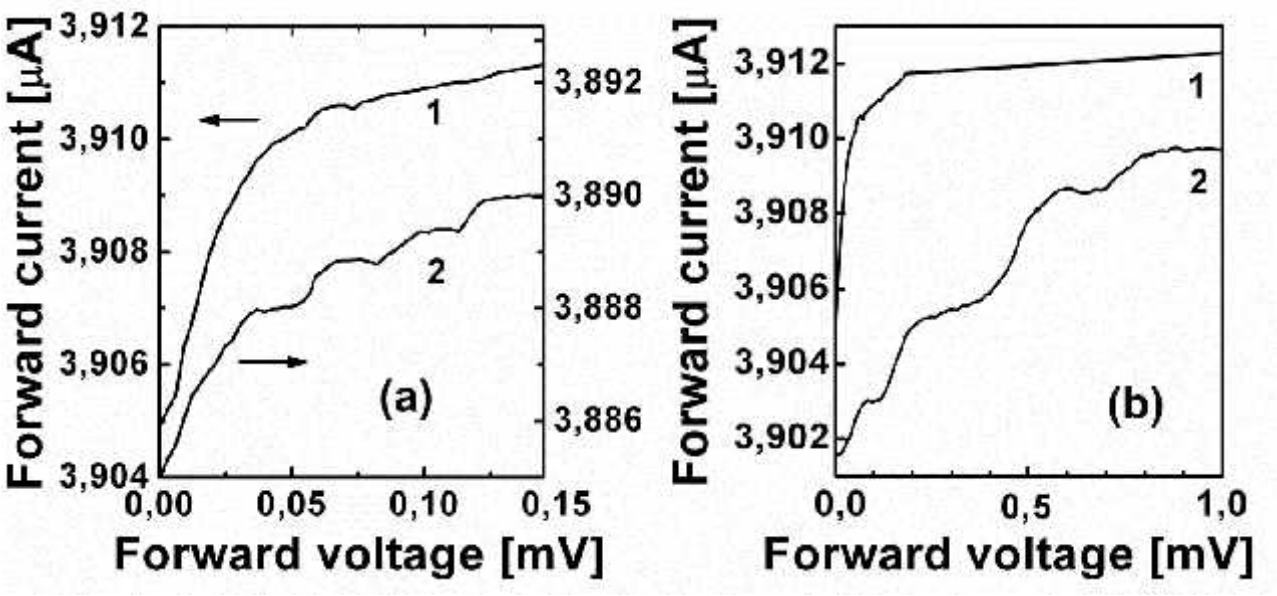

Fig. 9. The Shapiro steps in the Josephson CV characteristics of the S-Si-QW-S sandwich structures that reveal by stepwise varying the GHz frequency generation at 9.3 GHz (a) and 120 GHz (b). The level of the drain-source current in both device structures was stabilized at the value of 10 nA.

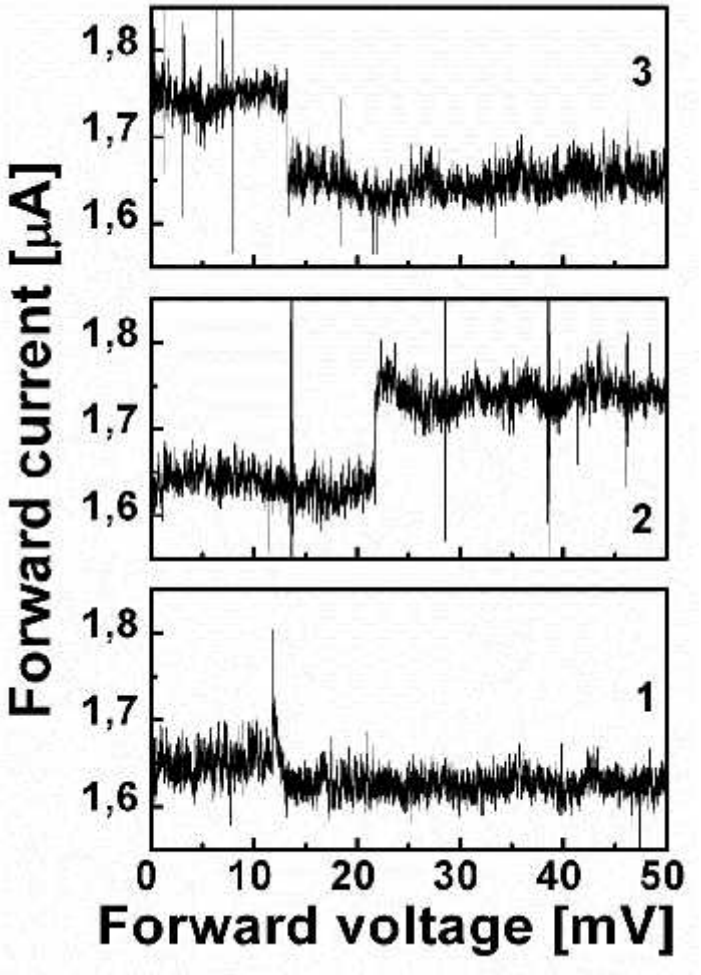

Fig. 10. The Shapiro steps in the Josephson CV characteristics of the S-Si-QW-S sandwich structures that reveal by stepwise varying the THz frequency generation at 5.3 THz (negative step) and 10.6 THz (positive step) which is caused by forming the superconductor gap. The level of the drain-source current in the recorder was stabilized at the value of 10 nA, while in the source the drain-source current was subsequently varied; 1 – I_{ds}=10 nA, 2 – 1 μA, 3 – 50 μA.

Thus, the technique presented identifies the GHz generation, which appears in the S-Si-QW-S structure under applied voltage thereby giving rise to the EDESR measurements of single impurity centers without using the hf-source and recorder. In principle the same generation is able to be induced also under illumination as a result of the transitions between subbands of the 2D holes, thus resulting in the possibilities of the ODMR measurements.

Besides, similar device has been prepared within frameworks of the planar technology on the n-type 6H-SiC (0001) wafer doped with nitrogen at the concentration of 5 10^{18} cm^{-3}. Firstly, the pyrolysis of silane was used to obtain the oxide overlayer on the 6H-SiC (0001) surface. Then, the photolithography processes and subsequent etching were applied to make the Hall geometry windows (see Fig. 11a). Finally, the short-time diffusion of boron has been performed from the gas phase under controlled injection of the silicon vacancies at the temperature of T = 900^0C [32]. The shallow diffusion profiles of boron were measured using the SIMS technique that has revealed the important role of the low temperature dissociative vacancy diffusion mechanism due to excessive amount of the silicon vacancies generated by the 6H SiC-SiO_2 interface (Fig. 12a).

The quantum conductance and tunneling spectroscopy measurements have shown that the p+-diffusion profile obtained represents the ultra-narrow p-type quantum well (QW) confined by the δ-barriers heavily doped with boron, N(B) > 10^{21} cm^{-3} [32]. Moreover, the negative differential resistance appeared to be observed under the voltage applied both to the p+-n junction and along the device thereby verifying the correlation gap in the one-electron band scheme of the δ-barriers (see Fig. 13a). This correlation gap as well as the fall in the electrical activity of shallow boron acceptors contrary to high level of boron doping seems to result from the negative-U reconstruction, $2B^0 => B^+ + B^-$ along the c- axis (Figs. 11b and 12b).

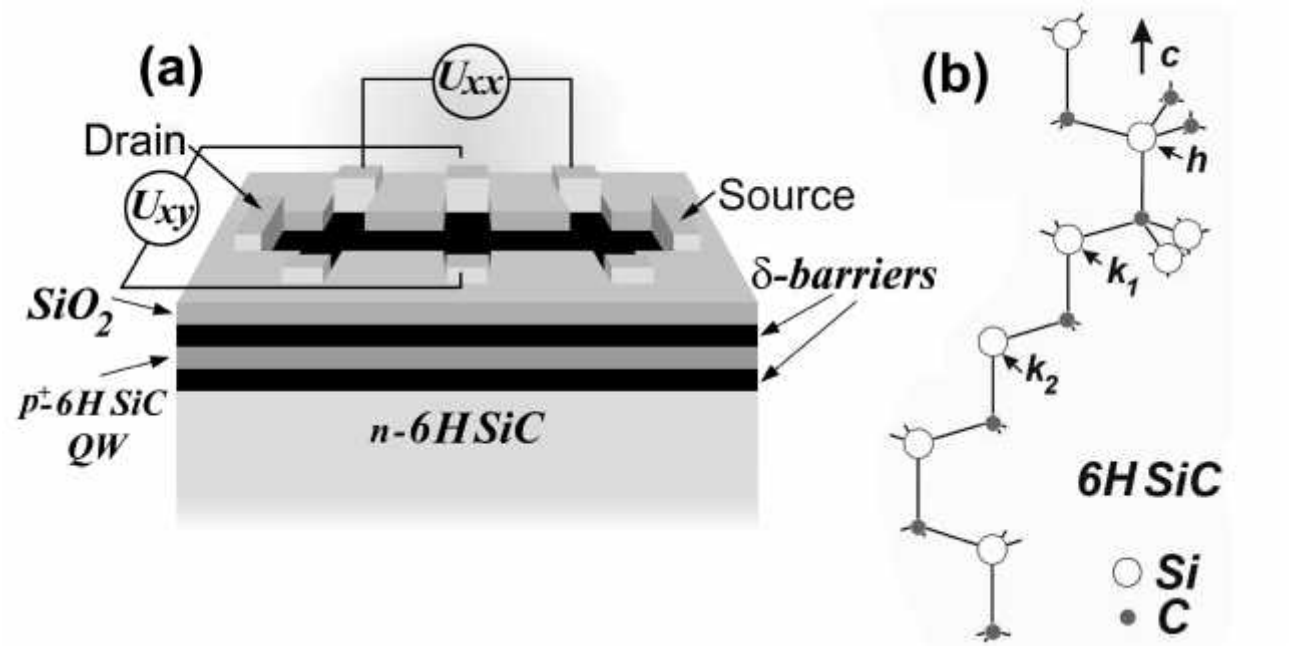

Fig. 11. (a) Device schematic, showing the perspective view of the 6H-SiC nanostructure performed within the frameworks of the Hall geometry. The 6H-SiC nanostructure represents the p-type 6H-SiC quantum well confined by the δ-barriers heavily doped with boron on the n-type 6H-SiC surface. The changes of the longitudinal, U_{xx}, and the transverse, U_{xy}, voltage are measured by varying the value of the external magnetic field when the drain-source current, I_{ds}, is stabilized at the extremely low value. (b) Silicon carbide polytype 6H-SiC.

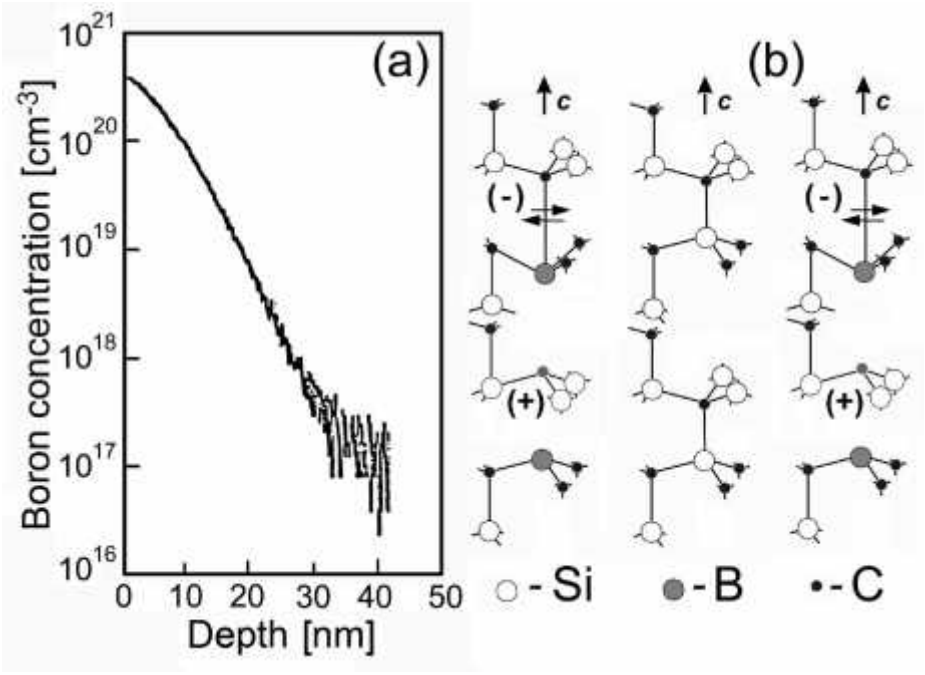

Fig. 12. (a) SIMS data for the p^+-boron diffusion profile on the n-type 6H SiC (0001) surface. The short-time diffusion of boron has been performed under controlled injection of silicon vacancies at the temperature of 900°C after previous oxidation using the pyrolysis of silane (b) Negative-U dipole boron centers in 6H-SiC; $2B^o \Rightarrow B^+ + B^-$.

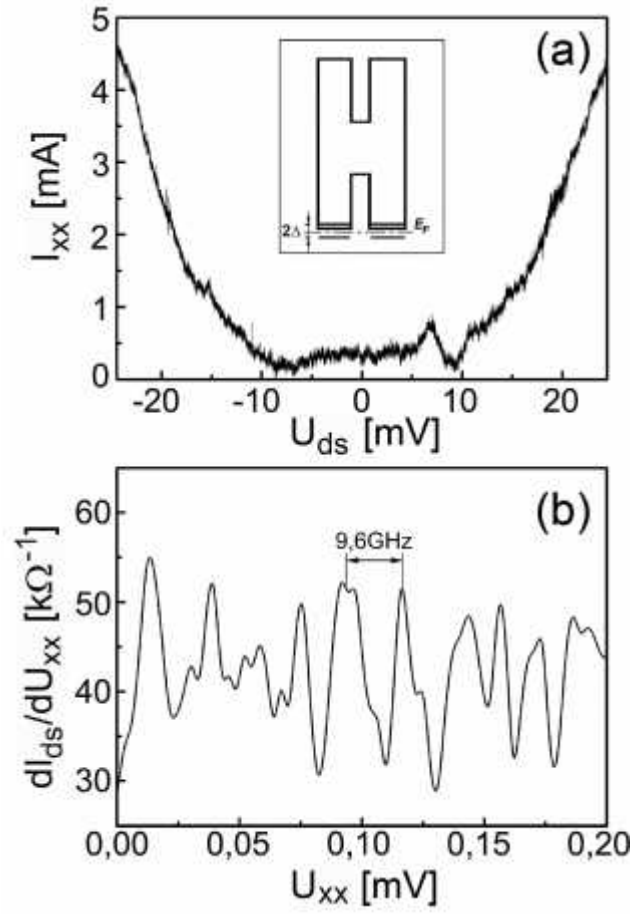

Fig. 13. Correlation energy gap in the one-electron band scheme of the 6H-SiC nanostructure that represents the p-type 6H-SiC quantum well confined by the δ-barriers heavily doped with boron on the n-type 6H-SiC surface. (a) The correlation energy gap in the valence band of the δ-barriers which is caused by forming the negative-U dipole boron centers, $2B^o \Rightarrow B^+ + B^-$, is revealed by measuring the longitudinal current-voltage characteristics, $I_{xx} = f(U_{ds})$, as a function of the positive and the negative values of drain-source voltage, U_{ds}, at the temperature of 77 K. The one-electron band scheme of the 6H-SiC nanostructure with the correlation gap near the valence band of the δ-barriers is shown in insert. (b) The oscillating dependence $dI_{ds}/dU_{xx} = f(U_{xx})$ that was measured by varying the values of the stabilized drain-source current at the temperature of 77 K appears to result from the GHz emission due to the excitation of the dipole boron centers in the δ-barriers. The frequency selection at the value of 9.6 GHz was used by varying the value of a load resistance and by incorporating the microcavities in the plane of the 6H-SiC nanostructure.

It should be noted that the dipole boron centers in 6H SiC similarly to the trigonal $B^+ + B^-$ pairs in silicon appeared to be the effective internal broadband source of the GHz and THz emission, with the frequency selection dependent on the characteristics of the n-type 6H SiC substrate as a load resistance (see Fig. 3b) [11, 33]. Therefore the δ-barriers heavily doped with boron substantially promote the electrically and optically detected ESR (EDESR and ODMR) techniques without application of the external hf source in low-dimensional semiconductor structures [3, 11, 13, 17]. In this case the internal hf emitter is able to excite the transitions between Zeeman sublevels of free carriers and single point defects under both drain-source and the p+-n junction bias voltage, thereby making possible the ESR measurements as the response of conductance or luminescence by varying the external magnetic field. Besides, to enhance the sensitivity of the EDESR and ODMR techniques, the special microcavities are incorporated into the plane of a nanostructure, with the sizes corresponding to the frequencies, $L=\lambda/2n$; where n is the refractive index, L is the microcavity size and λ is the wavelength of the GHz- and THz-radiation. Here the length of the δ-barrier area was picked up to satisfy to the selection of the frequency value of 9.6 GHz.

When inserted in a microcavity, the hf excited Zeeman system with two or more sublevels can be revealed in a weak or strong coupling regime. For weak coupling, the amplitude of ESR spectra can be enhanced or reduced by tuning the discrete microcavity modes in and out resonance conditions. By contrast, strong coupling is characterized by the reversible energy exchange between the microcavity mode and the hf induced Zeeman transitions, which is expected to result in the Rabi splitting in the ESR (EDESR and ODMR) spectra. This coherent coupling seems to be an analogue of well-known normal-mode coupling (NMC) regime caused by the microcavities embedded in a semiconductor nanostructure that is revealed by measuring a Rabi splitting in optical spectra as a consequence of anti-crossings between the quantum dot exciton and microcavity-mode dispersion relations [34].

In addition to the aforesaid, the contribution to the internal hf generation seem to be caused by the spin precession of the $B^+ + B^-$dipole moment that results in the Rabi oscillations and by the spin-dependent hole scattering on the negative-U dipole boron centers that appears to induce the Bloch oscillations. Besides, in the case of homogeneous distribution of the dipole boron centers, the δ-barriers have been shown to exhibit the properties of high temperature superconductors. Therefore the internal hf generation seems to result from the Josephson emission, with the frequency selection controlled by measuring the Shapiro steps [11].

Thus, the GHz emission from the δ-barriers appeared to be a basis of the new EDESR technique by measuring the dependences of the longitudinal, U_{xx}, and transverse, U_{xy}, voltages on the magnetic field value without the external hf source and recorder as well as the external cavity [11]. Here this EDESR technique was used to identify the silicon vacancy related centers in the planar 6H-SiC nanostructure that is not exposed to previous or subsequent e- and n- irradiation. Finally, contrary to minor amounts of centers, the N-V_{Si} defect was identified for the first time in the planar 6H-SiC nanostructure with the ESR Bruker ELEXSYS E580 spectrometer at 9.7 GHz in the temperature interval from 5K to 40K.

III. RESULTS

The phosphorus ESR lines with the characteristic hf splitting of 4.1 mT are observed, with a complicated behavior of intensities and phases due to effects of a spin-dependent scattering (Fig. 14 a and b). Besides, the spin-dependent scattering of 2D holes on the phosphorus shallow centers is revealed by measuring the phosphorus line splitting that is evidence of the exchange interaction, which is similar to the effect of zero-field splitting in one-dimensional channels [35, 36]. It should be noted that this considerable splitting of the P-lines has been found, for the first time, in the same device using the ordinary EDESR technique [13]. The high sensitivity of the new EDESR technique is confirmed by the measurements of the NL8 spectrum that identifies residual oxygen thermodonors, TD^+ state, in the

p-type Si-QW (Fig. 14 a and b) [37]. This center of the orthorhombic symmetry has been also found by the ordinary EDESR method in the sandwich structure discussed here [38]. The central lines in the EDESR spectrum are slightly different from the NL10 spectrum that is related to the neutral thermodonor containing a single hydrogen atom. Nevertheless, this EDESR spectrum appears to identify the hydrogen-related center in the p-type Si-QW, because its characteristic hf splitting, 23 MHz, corresponds to the hf hydrogen splitting [39]. Different phase of the hf lines that result from the hydrogen-related center is of importance to be noticed, which seems to result from the high spin polarization.

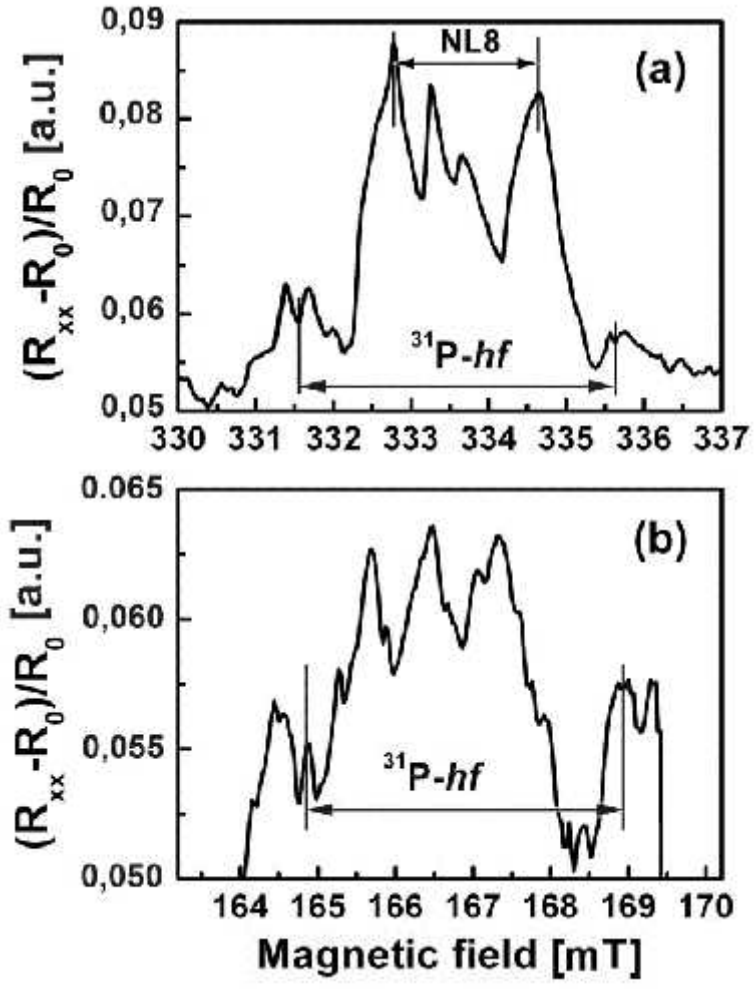

Fig. 14. (a) -EDESR of phosphorus, NL8 and hydrogen-related centers in the Si-QW confined by the superconductor δ-barriers, which is observed by measuring a magnetoresistance without the external cavity as well as the hf source and recorder. T=77 K. B||<100> in the plane ⊥ to the {100} interface. ν=9.3 GHz. The 23 MHz splitting revealed by the central lines seems to be evidence of the hf hydrogen structure. (b) – EDESR reply from the second harmonic.

The 23 MHz hf splitting is verified also in the EDESR line with a g-value of 2.07 like Fe^0 in bulk silicon (Fig. 15 a). This EDESR spectrum is of interest to exhibit a strong angular dependence of the line intensity with maximum for B||<111> that is practically the same as for the iron-related center identified by the ordinary EDESR, with the observation of the double quantum transitions (Fig. 15 b) [13, 38]. The EDESR spectrum shown in Fig. 15 b is not related however to the well-known FeH center [40] and seems to be a result of the hydrogen passivation of interstitial Fe^0 center.

The high sensitivity of the EDESR technique demonstrated below allows the studies in weak magnetic fields that are of importance for the measurements of the hf splitting for the centers inserted in the quantum wells, which are characterized by the large g-values. Firstly, this advantage is revealed by measuring the EDESR spectrum of the Fe^+ center, which appears to exhibit the hf ^{29}Si splitting in the absence of the external cavity as well as the hf source and recorder (Fig. 15c).

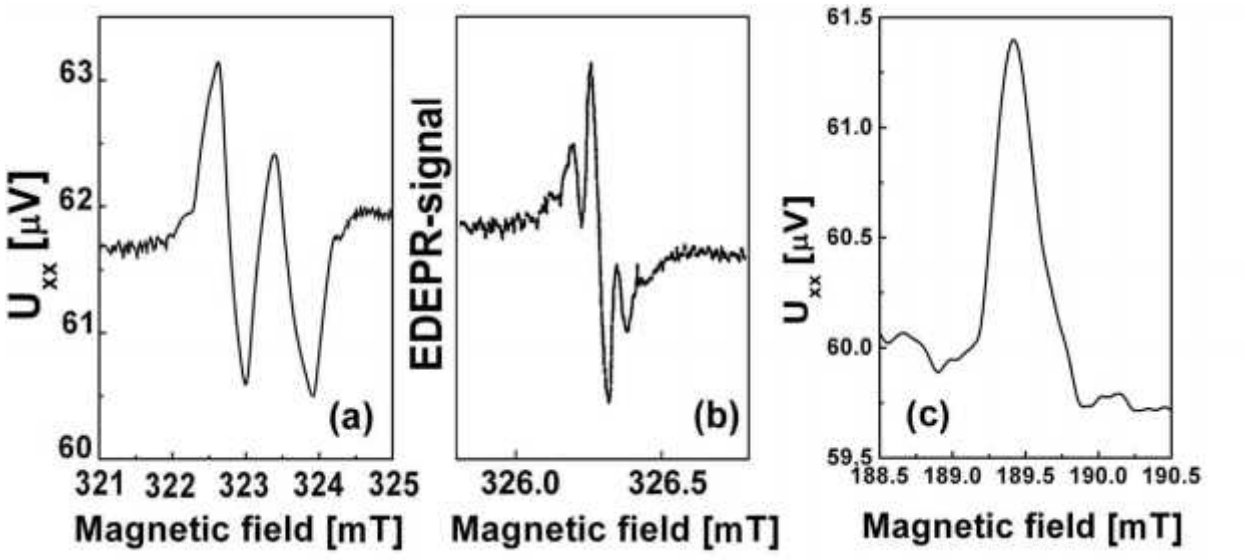

Fig. 15. (a) EDESR of a FeH-related center in the Si-QW confined by the superconductor δ-barriers, which is observed by measuring a magnetoresistance without the external cavity as well as the hf source and recorder. T=77 K. B||<100> in the plane ⊥ to the {100} interface. ν=9.3 GHz. The 23 MHz splitting seems to be caused by the HFI with hydrogen. (b) The hf structure of the X-line observed with ordinary EDESR at 50mW and low modulation amplitude (0.05mT); T=3.7K. B || <111>, 50 scans [13, 38]. (c) EDESR of the Fe^+ center in the Si-QW confined by the superconductor δ-barriers, which is observed by measuring a magnetoresistance without the external cavity as well as the hf source and recorder. T=77 K. B||<100> in the plane ⊥ to the {100} interface. ν=9.3 GHz.

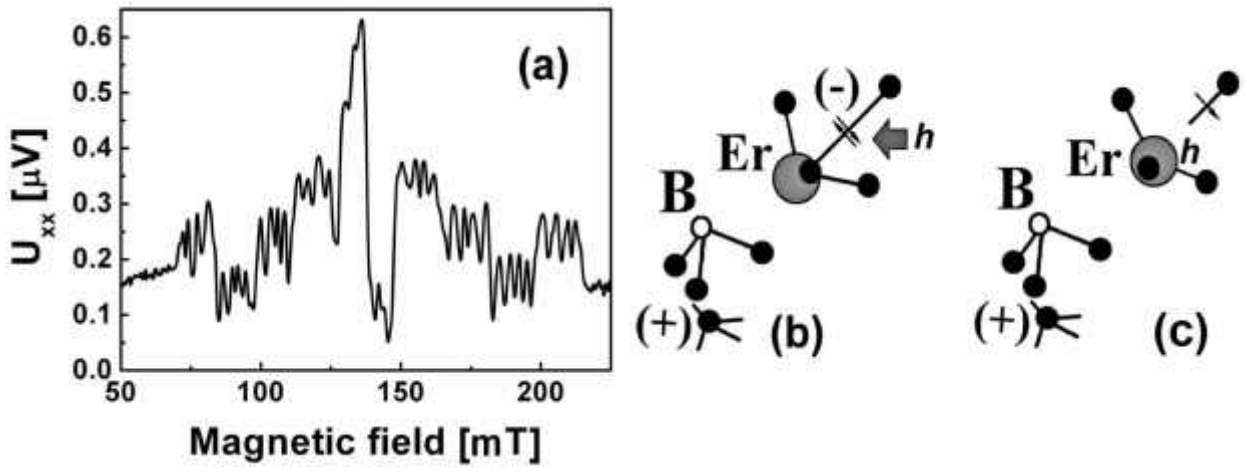

Fig. 16. (a) EDESR of the trigonal Er-related center in the Si-QW confined by the superconductor δ-barriers, which is observed by measuring a magnetoresistance without the external cavity as well as the hf source and recorder. T=77 K. B||<100> in the plane ⊥ to the {100} interface. ν=9.3 GHz. The hf erbium structure (I=7/2) are split in four lines that seem to be due to the presence of boron (I=3/2) inside of the Er-related center. Model for the trigonal dipole boron-erbium center (b), with paramagnetic state created by the capture of 2D holes in the Si-QW confined by the superconductor δ-barriers (c).

Secondly, the hf structure of the erbium-related center is found, for the first time, in silicon (Fig. 16a). Erbium doping was done at the diffusion temperature of 1100°C in the process of long-time

diffusion accompanied by surface injection of vacancies from the interface between the oxide overlayer and the n-type Si (100) substrate. Then, the sandwich structure that represents the p-type Si-QW confined by the superconductor δ-barriers was prepared on the n-type Si (100) (Fig. 1). Thus, small concentration of the erbium-related centers is a basis of the EDESR and ODMR observation that are caused by the spin-dependent scattering of 2D holes. The g-value, 4.82, and the trigonal symmetry of the erbium-related center identified from the angular dependences of the EDESR spectrum observed are evidence of its similarity to the erbium center studied by the ordinary ESR [41]. The components of the hf erbium structure, I=7/2, are seen to be split in four lines (Figs. 16 b and c). This splitting seems to result from the hf structure of boron (I=3/2) that forms the trigonal dipole centers in the δ-barriers. The results obtained allow the model of the erbium-related center in the p-type Si-QW within frameworks of the replacement of one boron atom in the trigonal dipole center by erbium thereby forming single dipole centers B^{+}-Er^{-} (Fig. 16 b). The paramagnetic state of this center seems to be created by the capture of 2D holes (Fig. 16 c) transferred along the edge channels in the sandwich structures.

Since the measurements of the magnetoresistance were performed without any light illumination and injection of carriers from the contacts, the EDESR effects appear to result from the spin-dependent scattering of spin-polarized holes from a single paramagnetic center or a few such centers in the edge channels of the S-Si-QW-S sandwich structures. The spin polarization of holes is caused by of the multiple Andreev reflection between the two B-doped sheets confined by the superconductor δ-barriers [2]. It has to be emphasized that the spin-polarized free 2D holes perform a quantum diffusive motion due to elastic scattering on a static random potential in the edge channels. This elastic scattering is not spin-dependent, and the phase of the hole wave function accumulates a purely geometric contribution, while the phase memory remains conserved. Thus, the weak localization regime of the hole transport is achieved. The hole phase memory is well known to allow the destruction due to the inelastic electron-electron and/or electron-phonon interactions. The corresponding characteristic time is denoted by τ_{φ}. If the external magnetic field is applied, the following two additional contributions to the hole wave function phase appear. The first one is the Aharonov-Bohm contribution which is spin independent and proportional to the magnetic flux through the cross section of the diffusive trajectory. This contribution is phase conserving. The second spin-dependent phase contribution is due to spin dependent magnetic-impurity scattering of 2D holes. This contribution might break the phase memory, and the interrelation of its characteristic time with τ_{φ} is important. However, this type of magnetic-impurity scattering is not a direct scattering process of the holes but rather the cumulative influence of the magnetic field of a given paramagnetic center on the diffusive hole phase through the hole-center spin-exchange interaction. It should be noted that a direct scattering process might significantly reduce the conductance of the edge channel. So it is reasonable to assume some spacing, of about 1-3 nm, between the paramagnetic center and the edge channel preventing from the direct scattering of the holes. Indeed, recent experimental data demonstrate directly the existence of such nearby centers that produce random telegraph signal of various nature in some diode structures. In the sandwich structure under consideration we observed several types of paramagnetic centers with similar random influence on the hole wave function phase. The magnetic random signals produced by the given center can be of the telegraph or shot noise nature and correspond to a temporal sequence of signals of alternative signs that appear at random moments. In any case of the noise statistics, the additional time-dependent phase accumulated by the hole wave function represents a random process with an exponential relaxation function. The corresponding correlation time, τ_s, is the characteristic of the ESR from the center considered. This is the mean time of spin-flip transitions at the center which is very sensitive to the deviation of the external magnetic field from its resonance value. Therefore the spin-dependent magnetic-impurity scattering of spin-polarized holes, described above, can be

accounted for in terms of the theory of weak localization in disordered structures that gives rise to the following generalized relationship for the positive magnetoresistance response caused by the EDESR saturation (Figs. 17 a and b) [42, 43]:

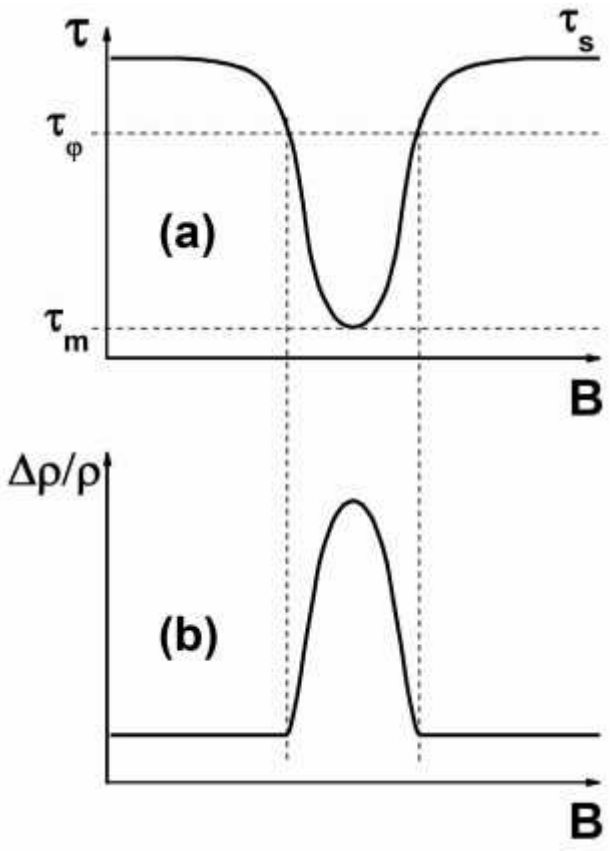

Fig. 17. The ESR reply in the conductance due to the spin-dependent scattering of carriers from single centers in the sandwich structures, which appear to result from the resonance behavior of the spin relaxation time within frameworks of a weak localization regime (a), with giving rise to the positive magnetoresistance (b).

$$\frac{\Delta\rho}{\rho}=\text{const}\int_{\tau_m}^{\tau_\varphi}\frac{dt}{t^{d/2}}\left\langle \exp\left(i\frac{4\pi e}{hc}\oint \vec{A}\times d\vec{l}-is_x\int_0^t \delta\omega(t')dt'\right)\right\rangle \quad (1)$$

where τ_m is the momentum relaxation time, τ_φ is the inelastic or phase relaxation time; τ_s serves here as the spin relaxation time of holes in the edge channels.

The spin relaxation of holes in magnetic fields outside the magnetic resonance range is determined by the random spin rotation that results in the spin delocalization: $\tau_s>\tau_\varphi>\tau_m$, whereas under the ESR saturation that is described by the second term in (1) results in a significant drop of the τ_s value and corresponding positive reply of magnetoresistance (Figs. 17 a and b):

$$\frac{\Delta\rho}{\rho}=\text{const}\cdot\cos\left(2\pi\frac{\Phi}{\Phi_0}\right)\cdot\int_{\tau_m}^{\tau_\varphi}\frac{dt}{t^{d/2}}\cdot\exp\left(-M_2\int_0^t (t-t')\Psi_{xx}(t')dt'\right) \quad (2)$$

where $\Psi_{xx}(t)=\exp\left(-\frac{|t|}{\tau_s}\right)$ is the relaxation function of ESR of the paramagnetic center; $M_2: J^2\langle s^2\rangle$ is defined by the exchange interaction between the hole and the paramagnetic center nearest to the hole diffusive closed trajectory in the channel. Equation (2) describes the positive

magnetoresistance effect observed under the ESR saturation as a response that is able to regenerate the weak localization regime which becomes destructive in the region far from ESR because of the random spin relaxation processes. The physical origin of this effect is due quantum interference of the two hole states corresponding to direct and inverse motion of the hole along the closed diffusive path in the static random potential in the channel. This is the reason why this magnetoresistance effect is very sensitive to the concentrations of even uncontrollable impurities. On the basis of presented arguments, the resonant positive magnetoresistance effect is accounted for as follows:

a) The exponential factor $\exp\left(-\frac{M_2 t^2}{2}\right)$ in (2) becomes dominant when the weak antilocalization regime becomes unstable due to generation and accumulation of a low frequency paramagnetic noise at the location of the diffusive hole in the edge channel; this case is described with the inequality $\tau_s > \tau_\varphi > \tau_m$.

b) The exponential factor $\exp\left(-M_2 t \tau_s\right)$ in (2) is different from the previous form and prevalent under the ESR saturation conditions resulting in the positive magnetoresistance response; this case is described with the inverse inequality $\tau_m > \tau_s > \tau_\varphi$; $L_{..} = \sqrt{D\tau_{..}}$ is the phase relaxation length, D is diffusion coefficient, $D = v_F^2 \tau_m / 2$, v_F is the Fermi velocity.

Finally, the new type EDESR effect has been additionally verified by the observation of the same ESR spectrum under the conditions of the second harmonic generation (see Fig. 14 b).

Figs. 17 shows two transmission spectra. The first one was obtained for silicon wafer before the boron diffusion. Several lines marked with “C-H” are demonstrated, which appear to result from the carbon-hydrogen acceptor center photoluminescence and its phonon replicas [44].

Several new lines in the transmission spectrum were observed in the same sample after the diffusion of boron that gives rise to the formation of the sandwich nanostructure discussed above (see the curve 2 in Fig. 18). Two strong lines observed in the 925 – 935 meV range and two lines in the 950 – 960 meV range seem to result from the luminescence of a heavy hole (hh) and light hole (lh) bound exciton at the Fe-B pair center [45]. The creation of this center is due to the residual Fe content.

The strong luminescence observed in the 925 – 935 meV range appears to be caused by the normal-mode coupling (NMC) of the hh exciton bounded at the Fe-B center and the photon mode of the microcavites which are created between self-assembled microdefects (Fig. 5). The NMC regime is revealed by the creation of absorption lines marked with arrows in Fig. 18, with the demonstration of the angular dependent Rabi splitting [1, 4, 5]. The common origin of these lines related to the Fe-B center results from the same fine structure in both absorption and luminescence part of the transmission spectrum seen in Fig. 19. The angular dependencies of the luminescence part of the transmission spectrum that is enhanced in the range of Rabi splitting allow its identification as the ODMR spectrum from the trigonal Fe-B pair [1, 4, 5].

Two silicon microcavities are revealed by the angular resolved transmission spectra that exhibit the excitonic NMC regime with the Si-QW confined by the δ-barriers heavily doped with boron in the spectral range of the Rabi splitting at T=300 K (Fig. 20 a) [46, 47]. The angular resolved measurements have revealed the strong coupling regime by an anti-crossing behavior between polariton states in the microcavity embedded in the Si-QW containing the carbon-hydrogen acceptor centers [48]. The NMC regime is found to give rise to the enhancement of bound exciton absorption (Fig. 20) and photoluminescence (Fig. 21) in the spectral range of the Rabi splitting. Moreover, the exciton localization at the carbon-hydrogen acceptor centers appeared to cause the giant triplet-singlet splitting in the absence of the external magnetic field which is created by strong coupling of the impurity states with the s-p electronic states of the host Si-QW (Figs. 20a and 21a). This strong sp-impurity states

mixing is revealed by the angular resolved absorption and photoluminescence that seem to reveal the ODMR spectra in zero magnetic field under the NMC conditions (Figs. 20b and 21b), because the ESR frequency is able to be selected from the THz range generated by the δ-barriers confining the Si-QW being in self-agreement with the splitting of the triplet sublevels in the exchange field induced by the bound exciton (Figs. 20c and 21c) [1, 4, 5].

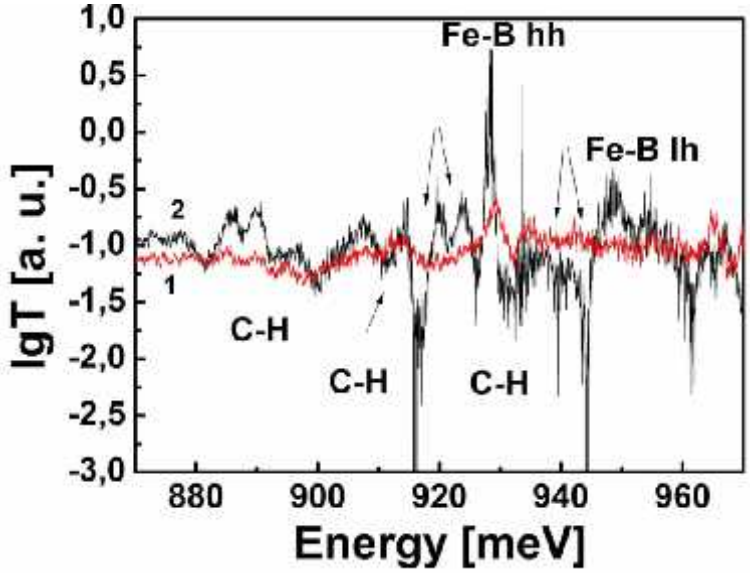

Fig. 18. Spectral dependences of the common logarithm of the sample light transmission coefficient: 1 (red) is related to device structure before the diffusion of boron; 2 (black) is related to the same device structure after the boron diffusion that results in the formation of the S-Si-QW-S sandwich. The Rabi splitting demonstrates at T=300K the excitonic normal-mode coupling with the Si-QW containing the Fe-B pairs being incorporated in the 1λ microcavity.

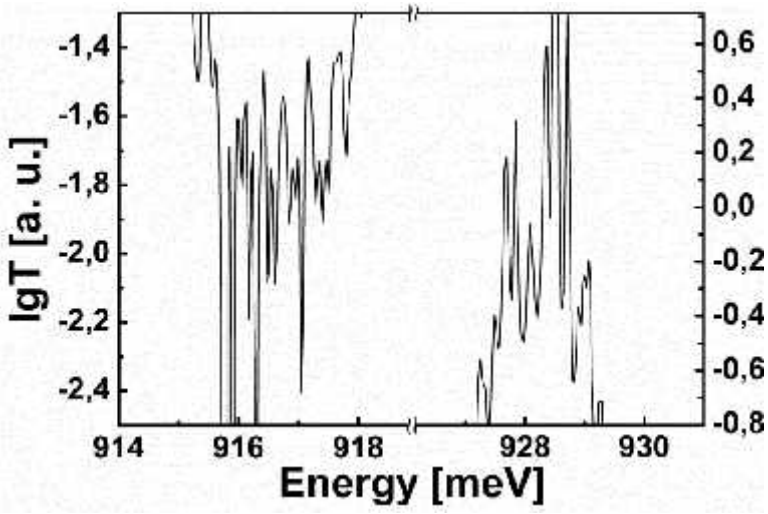

Fig. 19. Spectral dependences of the common logarithm of the light transmission coefficient that demonstrates the same fine structure of the lines arising from the excitonic normal-mode coupling regime in the S-Si-QW-S sandwich structure containing the Fe-B pairs.

Two different carbon-hydrogen acceptor centers, Cs-Ci-H [48], have been identified by measuring the ODMR spectra. The first center that is sensitive to the frequency value of 120 GHz seems to be associated with the presence of the E_c - 0.37 eV acceptor level which appears to give rise to the M-line 760.8 meV photoluminescence (Figs. 20a and c) [49]. The bound exciton absorption is predominant in the ODMR spectrum, because the energy of optical transition from the HH1 subband of 2D holes to the E_c - 0.37 eV acceptor level appears to be in resonance with the HH3-HH1 optical transition in the Si-QW. It should be noted that the double quantum transitions seem to be exhibited in the ODMR spectrum (Fig. 20a). The second center that is sensitive to the frequency value of 87 GHz seems to be associated with the presence of the E_c - 0.2 eV acceptor level which appears to give rise to the H-line 925.6 meV photoluminescence (Fig. 20) [44]. The phonon replica are observed in the photoluminescence spectrum that reveals also the giant triplet-singlet splitting, 5 meV. The multi-quantum transitions are seen to contribute to the ODMR spectrum (Fig. 21b). Finally, the

frequency values of 120 GHz and 87 GHz revealed by the modulation of the transmission spectra correlate with the splitting of the triplet sublevels in the exchange field induced by the bound exciton which appears to result from the ODMR spectra.

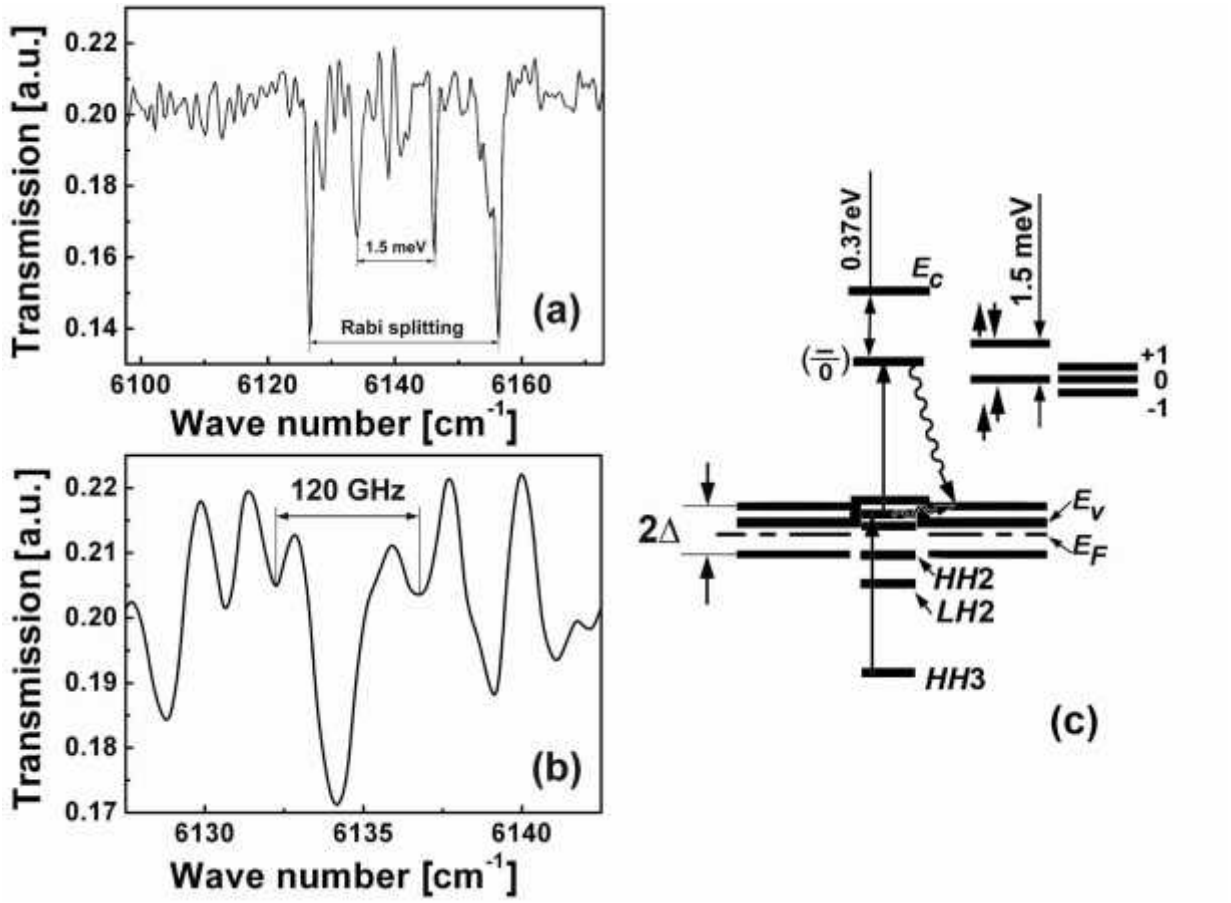

Fig. 20. (a) Spectral dependences of the light transmission coefficient that demonstrates at T=300K the excitonic normal-mode coupling with the Si-QW containing the carbon-hydrogen acceptor center being incorporated in the 1λ microcavity. (b) The giant triplet-singlet splitting revealed by the NMC regime allows the ODMR spectrum (120 GHz) by the triplet sublevel absorption of the bound exciton at the carbon-hydrogen acceptor center.
(c) The one-electron band scheme of the p-type Si-QW confined by the HTS δ-barriers that contains the carbon-hydrogen acceptor center. The bound exciton created at this center under optical pumping results in the giant triplet-singlet splitting. The presence of the Ec - 0.37 eV acceptor level appears to be associated with the M-line 760.8 meV photoluminescence [49].

The EDESR spectra of the isolated silicon vacancy centers that have been formed in the process of the preparation of the 6H-SiC planar nanostructure are shown in Figs. 22 and 23. These spectra were observed by measuring the only longitudinal or Hall magnetoresistance without the external cavity as well as the external hf source and recorder at the temperature of T=77 K, **B** || **c**, the frequency of the internal hf generation was equal to ν =9.6 GHz, and the drain-source current was stabilized at the value of I_{ds} = 10nA. The Rabi splitting is demonstrated when the field dependent U_{xy} voltage is registered, which is attributed to the normal-mode coupling (NMC) with the isolated vacancy center embedded in the microcavity that is incorporated in the 6H-SiC planar nanostructure. The lack of the Rabi splitting in the EDESR spectrum observed by measuring the U_{xx} voltage seems to be evidence of very high

sensitivity of the strong coupling regime to the relation between the coherence length and the mutual arrangements of contact areas. The role of the edge channels in the relative contribution of the weak and strong coupling to the EDESR signal is also needed to be taken into account.

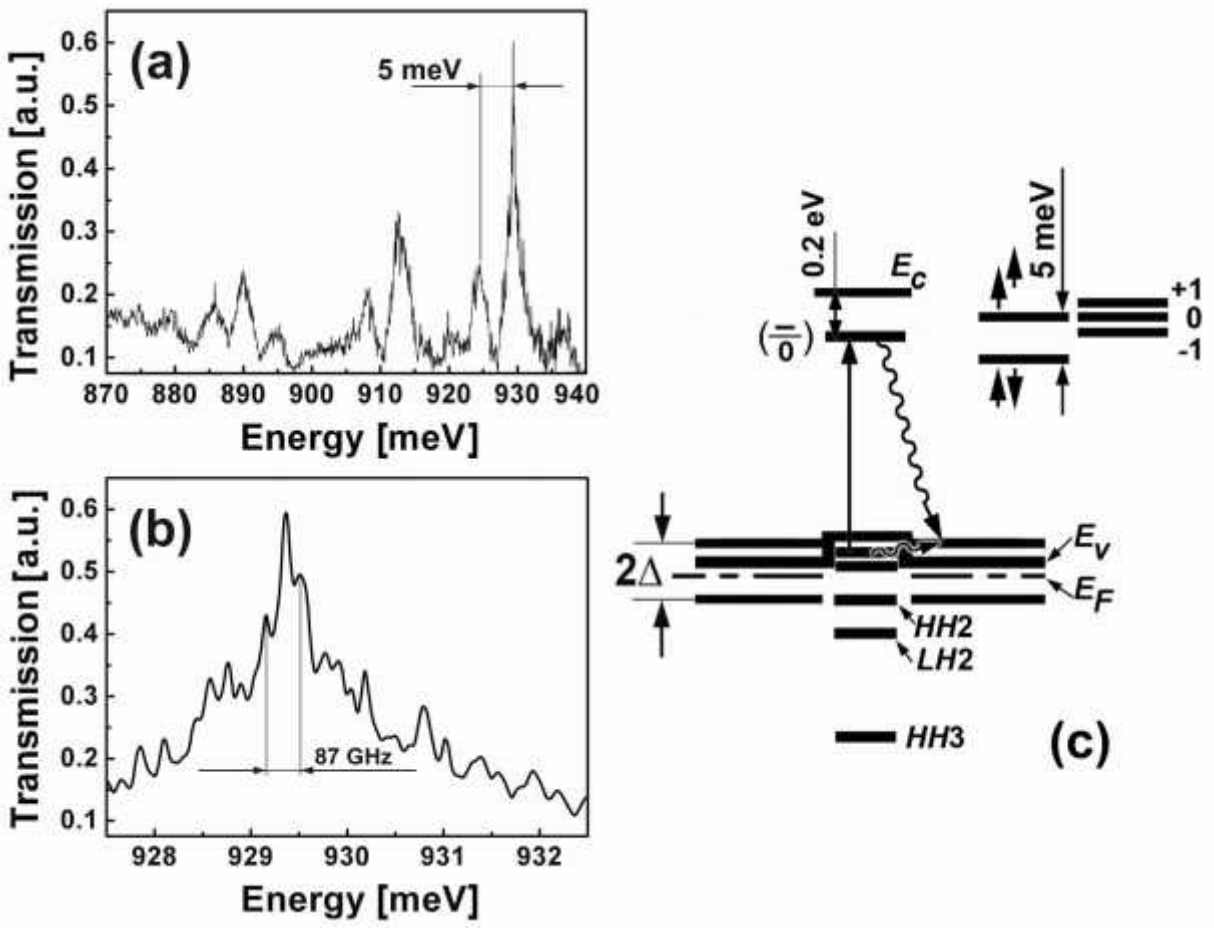

Fig. 21. (a) Spectral dependences of the light transmission coefficient that demonstrates at T=300K the excitonic normal-mode coupling with the Si-QW containing the carbon-hydrogen acceptor center being incorporated in the 1λ microcavity. (b) The giant triplet-singlet splitting revealed by the NMC regime allows the ODMR spectrum (87 GHz) by the triplet sublevel photoluminescence of the bound exciton at the carbon-hydrogen acceptor center. (c) The one-electron band scheme of the p-type Si-QW confined by the HTS δ-barriers that contains the carbon-hydrogen acceptor center. The bound exciton created at this center under optical pumping results in the giant triplet-singlet splitting. The presence of the E_c - 0.2 eV acceptor level appears to be associated with the H-line 925.6 meV photoluminescence [44].

The EDESR spectra shown in Figs. 22 and 23 appear to be in a good agreement with the data obtained by the X-band ESR and EDESR standard methods in the studies of the isolated silicon vacancy centers created under e-irradiation in the 6H-SiC bulk sample [50, 51]. In particular, the central line in Figs. 4 and 5 marked by V_{Si}^- is attributed to the negatively charged silicon vacancy with S = 3/2, whereas the lines indicated by V_{Si}^0(h) and $V_{Si}^0(k_1,k_2)$ are related to the neutral charge silicon vacancy but in different positions in the crystalline lattice. Symbols “h” and “k_1, k_2” depict the hexagonal and the quasi-cubic positions in the 6H-SiC crystal that has a hexagonal symmetry with the symmetry axis **c** (see Figs. 11b and 12b). It should be noted that the different phase of the lines from the

triplet V_{Si}^{0}(h) center is evidence of non-equilibrium spin polarization that seems to be caused by the hf pumping from the δ-barriers heavily doped with boron.

The presence of the residual shallow boron centers in the EDESR spectrum are also worthy of notice, because the most boron dopants are involved in the formation of the negative-U dipole boron centers **(**see Figs. 22 and 23). This result appears to highlight the high sensitivity of the EDESR method used in both strong and weak coupling regimes which allows the identification of the single centers in semiconductor nanostructures. Since the measurements of the magnetoresistance were performed without any light illumination and injection of carriers from the contacts, the spin-dependent scattering of spin-polarized holes on the paramagnetic centers in the edge channels of the 6H-SiC planar nanostructure appear to underlie the mechanism of the EDESR method, with internal hf emission in the presence of a microcavity [11]. Therefore the EDESR sensitivity determined by the magnetoresistance response appears to be interpreted here in terms of the interference transition in the diffusive transport of free holes respectively between the weak anti-localization regime ($\tau_S>\tau_\varphi>\tau_m$) in the region far from the ESR of a paramagnetic point defect located inside the edge channel and the weak localization regime ($\tau_\varphi>\tau_S>\tau_m$) in the nearest region of the ESR of that defect [11]. It follows that the important condition to register this resonant magnetoresistance response is to stabilize the drain-source current at the value of lower than 10 nA, which provides the spin interference regimes in the edge channels. Except the aforesaid it is necessary to pay attention that the EDESR spectra shown in Figs. 22 and 23 were observed at the temperature of 77 K. This unusual result seems to be a consequence of sharp increase in the spin-lattice relaxation time of holes in the low-dimensional silicon structures [3, 11, 13]. Besides, the strong anisotropy of the spin-lattice relaxation time seems to result in the disappearance of the $V_{Si}^{0}(k_1,k_2)$ lines in the EDESR spectrum registered by measuring the field dependent U_{xx} voltage (see Fig. 23).

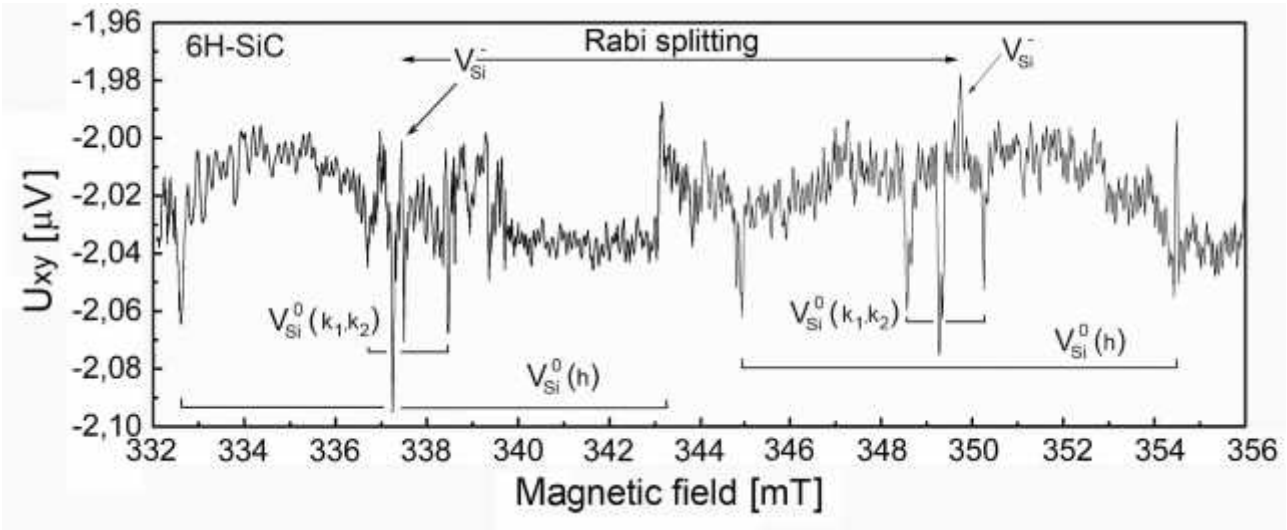

Fig. 22. The EDESR spectra of the isolated silicon vacancy centers in the p-type 6H-SiC-QW confined by the δ-barriers heavily doped with boron on the n-type 6H-SiC (0001) surface, which was observed by measuring the only Hall magnetoresistance without the external cavity as well as the external hf source and recorder. B||**c**, T=77 K, the frequency of the internal hf generation was equal to ν =9.6 GHz, and the drain-source current was stabilized at the value of I_{ds} = 10nA. The Rabi splitting is demonstrated, which is attributed to the normal-mode coupling (NMC) with the isolated vacancy center embedded in the microcavity that is incorporated in the 6H-SiC planar nanostructure.

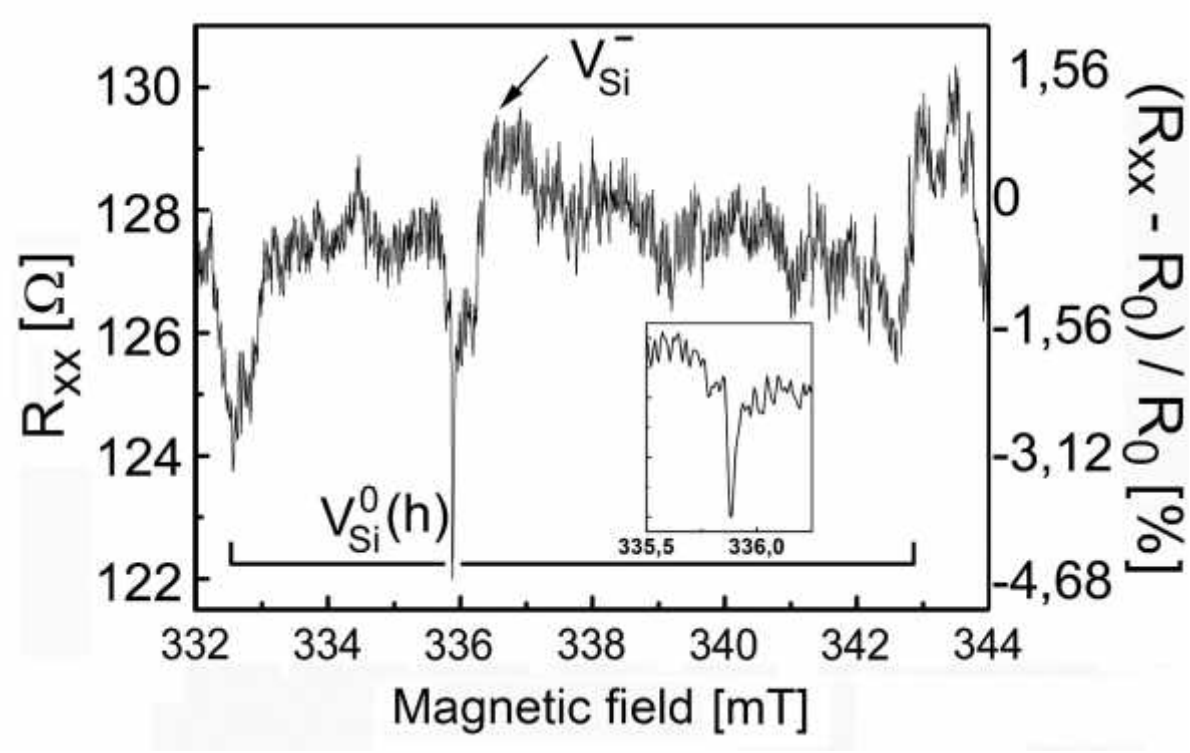

Fig. 23. The EDESR spectra of the isolated silicon vacancy centers in the p-type 6H-SiC-QW confined by the δ-barriers heavily doped with boron on the n-type 6H-SiC (0001) surface, which was observed by measuring the only longitudinal magnetoresistance without the external cavity as well as the external hf source and recorder. B ||c, T=77 K, the frequency of the internal hf generation was equal to ν =9.6 GHz, and the drain-source current was stabilized at the value of I_{ds} = 10nA. The EDESR spectrum of residual shallow boron centers in the 6H-SiC nanostructure is shown in insert.

The EDESR spectrum of the triplet N-V_{Si} defect (S=1) consists of two strong lines located at 250 mT and 450 mT (see Fig. 24). The high resolution of the EDESR method allowed the registration of the N-V_{Si} defect fine structure as a result of which the lines of spectra are divided into three lines due to nitrogen nuclear spin I=1, with the value of the hf splitting equal to 0.5 mT. The absence of the EDESR lines related to the nitrogen donor center is of importance to be noticed, which seems to result from the capture of silicon vacancies practically all of them in the area of the quantum well confined by the δ-barriers heavily doped with boron. Besides, the sensitive volume of the EDESR method is about several nanometers in the depth of the sample multiplied on Hall bar geometry area of the device structure that hinders with the identification of defects in the volume of the n-type 6H SiC (0001) wafer. However the EDESR method based on the registration of the negative or positive magnetoresistance in the weak localization regime under resonance conditions is highly sensitive inside the QW area [11]. In particular, the EDESR spectrum of the N-V_{Si} defect shown in Fig. 6 reflects the contribution from 5 10^4 centers taking account of the section area of the edge channels in the device structure, 2 nm x 2nm, while the ordinary ESR method allows signal detection minimum from 10^{10} spins.

This value corresponds to the maximum number of the N-V_{Si} defects which can be created by the capture of silicon vacancies on nitrogen donors in the process of the preparation of the device if to take into account the sizes of the doping area. This important condition allowed the ESR detection of the N-V_{Si} defect in the same device with the highly sensitive Bruker ELEXSYS E580 spectrometer (see Fig. 25a).

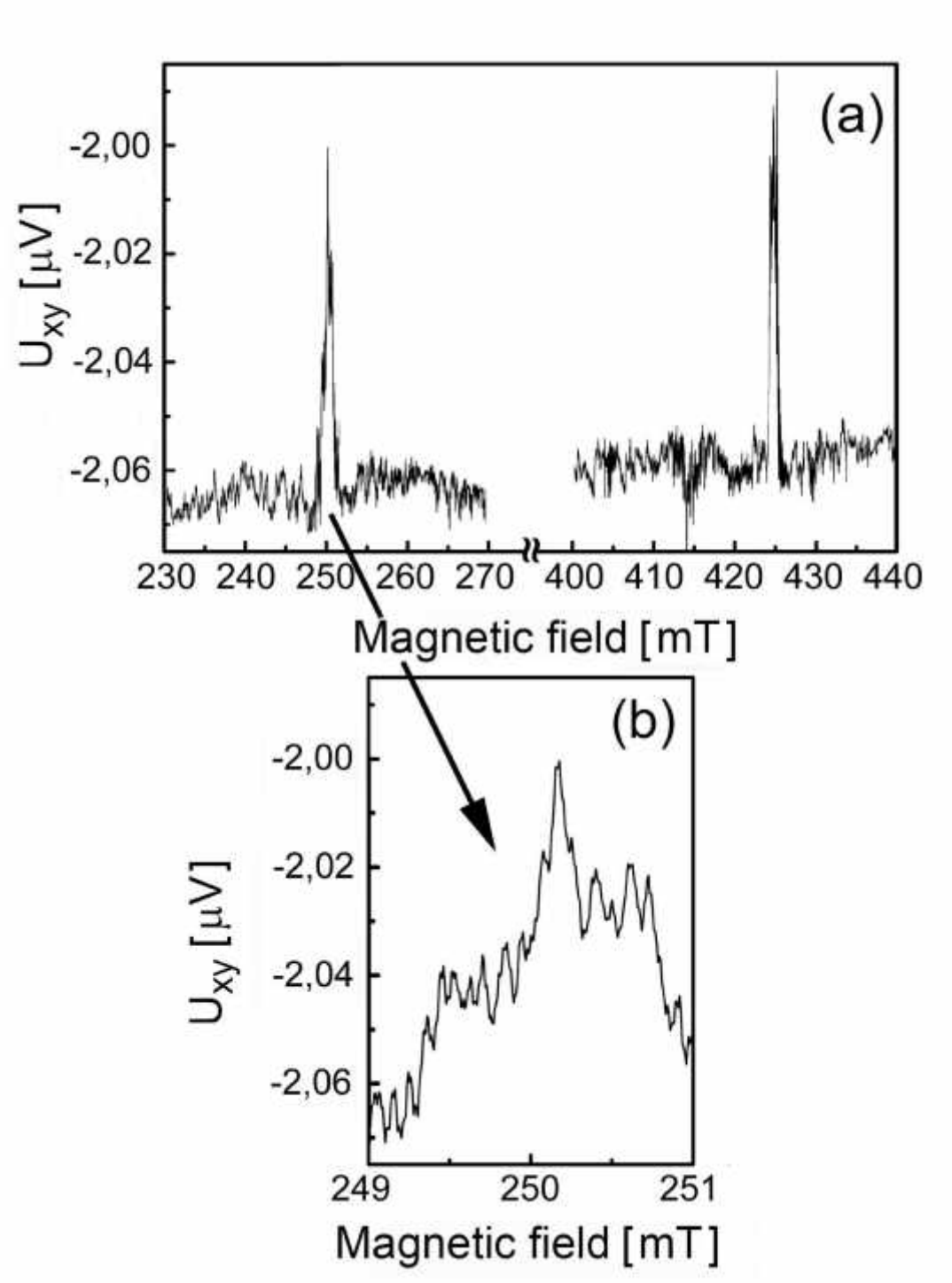

Fig. 24. The EDESR spectrum of the N-V_{Si} defect (S=1) observed in the p-type 6H-SiC-QW confined by the δ-barriers heavily doped with boron on the n-type 6H-SiC (0001) surface, which was observed by measuring the only Hall magnetoresistance without the external cavity as well as the external hf source and recorder. B $\|$ **c**, T=77 K. The frequency of the internal hf generation was equal to ν =9.6 GHz, and the drain-source current was stabilized at the value of I_{ds} = 10nA. Fine structure resolved in the EDESR spectrum appears to be evidence of the nitrogen presence (I=1). Isolated nitrogen donor centers inside the 6H-SiC nanostructure were absent as a result of interaction with silicon vacancies that seems to give rise to the formation of the N-V_{Si} defects.

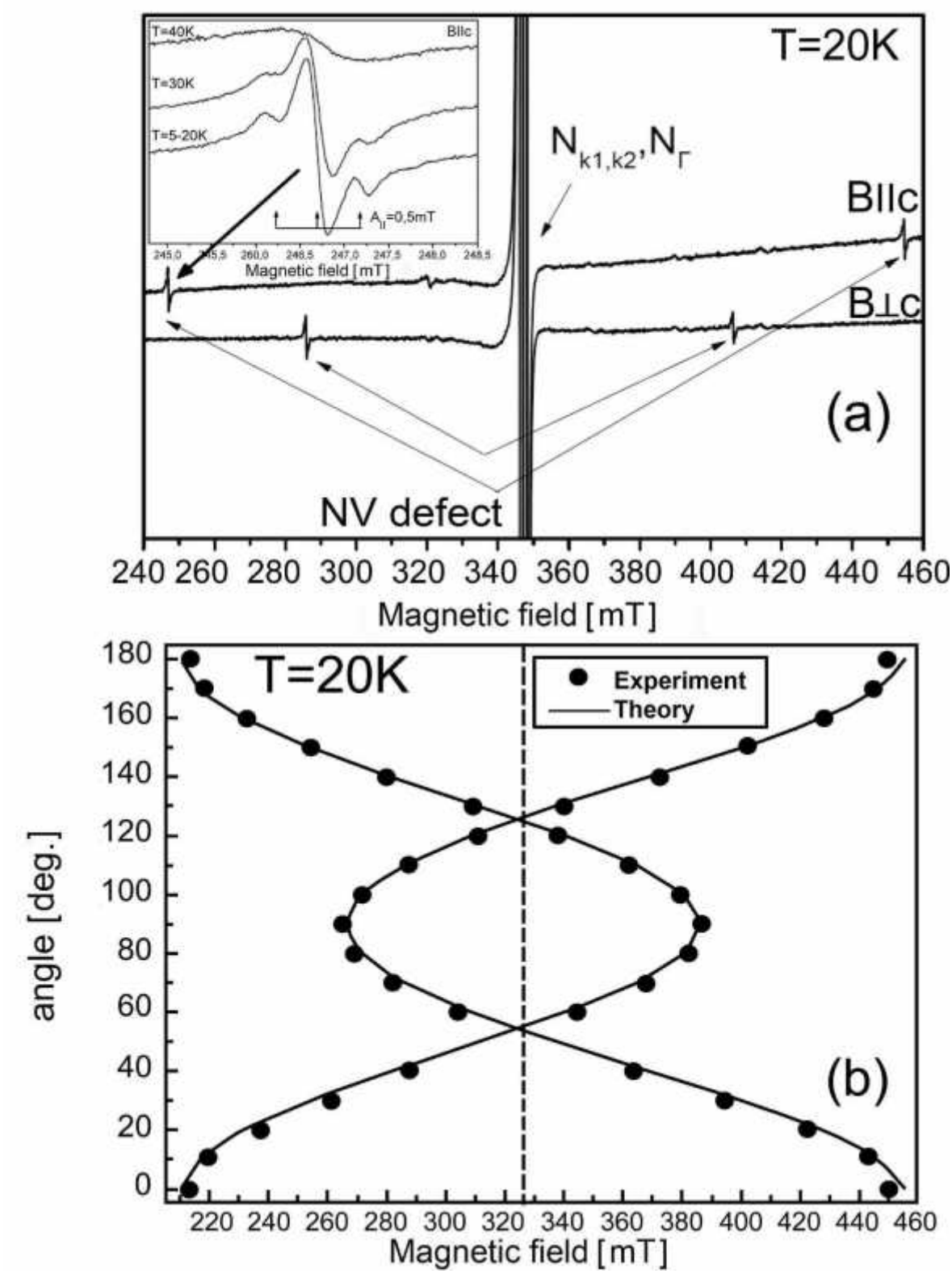

Fig. 25. The ESR spectrum (a) and the angular dependence of the *f*s structure constant D (b) of the triplet center observed in the p-type 6H-SiC-QW confined by the δ-barriers heavily doped with boron on the n-type 6H-SiC (0001) surface.
(a) The fine structure resolved in the ESR spectrum of a triplet center was shown in insertion. T=20K.
(b) The rotation of the magnetic field was in $(11\bar{2}0)$ plane.

In addition to the dominant spectrum of the nitrogen (N) donors substituting quasi-cubic ($N_{k1,k2}$) and hexagonal (N_h) sites originated from the n-type 6H-SiC (0001) bulk area, a fine structure (fs) doublet lines of small intensity with fs splitting of $\Delta B_{||}$=237.6 mT is observed in the temperature interval from 5K to 40K and related to the triplet center with S=1. The fact that the fs lines corresponding to the electron transitions (M_S=1=>M_S=0; M_S=–1=>M_S=0) were detected in darkness confirms a triplet ground state of the defect center. When the amplitude modulation of the magnetic field was taken smaller than the width of the triplet lines, as can be seen from figure 7a, three hyperfine (HF) lines can be well resolved in the ESR spectrum of the defect center with value of the HF splitting of about 0.5 mT. The presence of the three HF lines indicates its origin from the HF interaction with one ^{14}N nuclei (S=1/2 and I=1). Thus, triplet center seems to consist of the nitrogen atom and silicon vacancy introduced into the device in the process of its preparation. Since there are three nonequivalent positions for the impurities and defects in the 6H-SiC lattice, it is expected that this property is also attributed to the observed defect. Therefore different intensity of the central HF triplet line and sidelines in Fig. 25a can be explained by the contribution of the ESR spectrum due to the defect substituting hexagonal site in the central line, which has a smaller unresolved HF structure. From the ratio between the central and sidelines of the nitrogen triplet, it was concluded that the triplet with the HF splitting of the 0.5 mT value corresponds to the defect substituting one quasi-cubic position. The angular dependence of the ESR spectrum shown in Fig. 25b that was measured by the rotation of the magnetic field in the plane consisting of the c axis appears to demonstrate the angular variation characteristic for a spin S=1 center.

The experimental angular dependence of the effective g-factor of EPR spectrum one can obtain taking the half-sum of the resonance fields of two spectral components: $g_{eff}(\Theta) = 2h\omega_0/\beta(H_{-1} + H_{+1})$, where $g_{eff}(\Theta)$ is an effective anisotropic g factor of the center, H_{-1}, H_{+1} are the low-field and high-field components of the resonance field of ESR spectrum; ω_0 is the microwave field frequency. The obtained experimental angular dependence of the $g_{eff}(\Theta)$ plotted in figure 8 is described by the following expression:

$$g_{eff}(\Theta)=1.999 - 0.0174\cdot\cos(2\Theta) - 0.0124\cdot\cos(4\Theta). \quad (3)$$

The difference between the function describing the experimental curve in Fig. 26 and the axially symmetric angular dependence of the g factor expressed by $g = (g_{||}\cos^2\Theta + g_{\perp}\sin^2\Theta)^{1/2}$ arises from the last term in (3). Because of the large value of the fs splitting it was suggested that the second order of the crystalline field contributes into this term. Ignoring the term describing the HF interaction the spin Hamiltonian for the paramagnetic S = 1 center with axial crystalline field D and axial g-tensor ($g_{||}$, $g_{\perp}$) is described as:

$$\hat{H} = g_{||}H_zS_z + g_{\perp}(H_xS_x + H_yS_y) + D(S_z^2 - S(S+1)/3). \quad (4)$$

Since the crystal-field term is large, to analyze the parameters of the triplet center, the direct numerical diagonalization of the spin-Hamiltonian matrix was required. To this end the laboratory axes system was rotated so that the spin Hamiltonian may be written in a diagonal form in the applied magnetic field B_0 = (0, sinΘ, cosΘ).

$$\hat{H} = gH_{z'}S_{z'} + D_0(S_{z'}^2 - S(S+1)/3) - D_1(S_z(S_+ + S_-) + (S_+ + S_-)S_z) + D_2(S_+^2 + S_-^2)/2$$
$$D_0 = 0.5D\ (3g_\parallel^2 \cos^2(\theta)/g^2 - 1); \quad g^2 = g_\parallel^2 \cos^2(\theta) + g_\perp^2 \sin^2(\theta);$$
$$D_1 = D \cdot g_\parallel g_\perp \sin(2\theta)/(4g^2); D_2 = D \cdot g_\perp^2 \sin^2(\theta)/g^2 \quad .(5)$$

Then the secular equation for the eigenvalues of the $\hat{H}$ on the spin wave functions |-1>, |0>, |1> is given by:

$$\begin{vmatrix} g(\theta)H + D_0 - \varepsilon & d_1 & d_2 \\ d_1 & -\varepsilon & -d_1 \\ d_2 & -d_1 & -g(\theta)H + D_0 - \varepsilon \end{vmatrix} = 0 \quad (6)$$

where $d_1 = Dg_\parallel|g_\perp\sin(2\Theta)/(2\sqrt{2}g^2)$; $d_2 = 0.5D(g_\perp^2/g^2)\sin^2(\Theta)$.

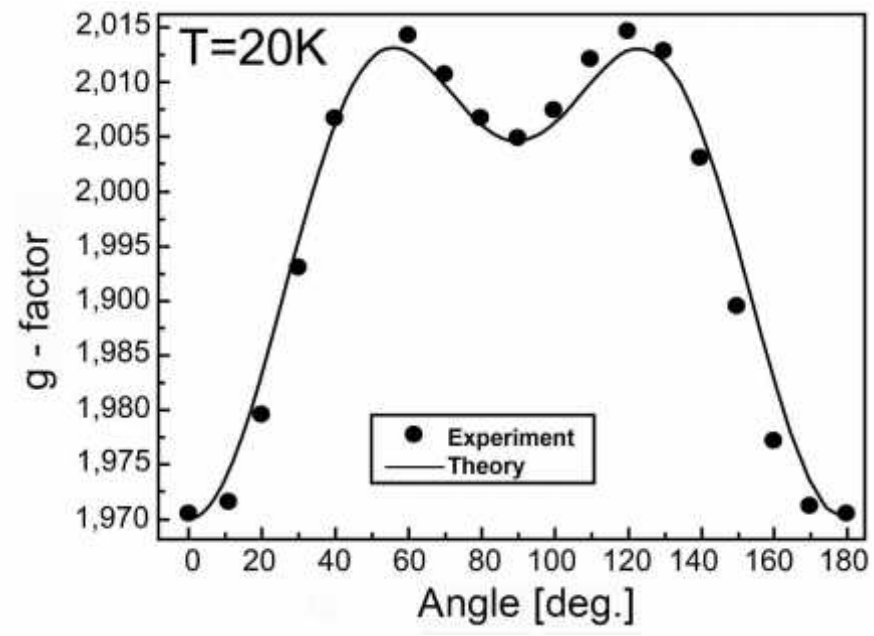

Fig. 26. Angular dependence of the $g_{eff}(\Theta)$ obtained from experiment and theory.

Solving (6) at an angle of $\Theta = 0$, we have found the constant of the crystalline field D = 120 mT and $g_\parallel$ = 1.9700. For the case of $\Theta = 90^o$, $d_1 = 0$; $d_2 = 0.5D$ the solution of (6) yields $g_\perp$ = 1.9964. With the values of $g_\parallel$, $g_\perp$, D the angular dependence of the g factor for arbitrary angle Θ can be obtained by the numerical calculation of the cubic equation derived from (6):

$$\varepsilon^3 - a\cdot\varepsilon^2 - b\,\varepsilon - c = 0 \quad (7)$$

where $a = 2D_0$; $b = (g^2H_{res}^2 + d_2^2 + 2d_1^2 - D_0^2)$; $c = 2D_0d_1^2 + 2d_1^2d_2$.

Because of the large value of the crystalline field constant D, the constant c in (7) cannot be neglected and the result of numerical calculation for $g_{eff}(\Theta) = \omega_0/(\beta H_{res})$, shown in Fig. 25b by the solid line, indicates that the term proportional to $\cos(4\Theta)$ in (3) arises from constant c. The parameters of the triplet center obtained from numerical diagonalization of the spin Hamiltonian are given in Tab. 1.

For comparison, the parameters of the N-V_{Si} triplet centers containing in their structure nitrogen atoms which were observed previously in electron (e) -irradiated (dose 10^{12}e/cm^2-10^{15}e/cm^2) and

annealed at T=900^{0}C synthetic diamond and in neutron (n) -irradiated (dose of 10^{21} cm^{-2}) n-type 6H-SiC after high temperature annealing at T=2000^{0}C were listed in Tab. 1.

Tab. 1. Parameters of the spin Hamiltonian for triplet centers observed in the 6H-SiC nanostructures, e-irradiated synthetic bulk diamond and n-irradiated bulk 6H-SiC of the n-type.

Center	**S**	**T/K**	***g***	**A/mT**	**D, 10^{-4} /cm^{-1}**	**Ref.**
N-V Diamond e-irradiated	1		g_{iso} = 2.0028	$A_{\parallel}$ = 0.082 $A_{\perp}$ = 0.075	960.7	[52]
N_C-V_{Si} 6H-SiC n-irradiated	1	3.5	g_{iso} = 2.003	$A_{\parallel}$ = 0.55	860	[53]
		70		$A_{\parallel}$ = 0.75 $A_{\perp}$ = 0.35	885	
N_C-V_{Si} 6H-SiC nanostructure	1	5-40	$g_{\parallel}$ = 1.9700(3) $g_{\perp}$ = 1.9961(3)	$A_{\parallel}$ = 0.55 $A_{\perp}$ = 0.45	1140	This work

As can be seen from Tab. 1, the observed triplet centers have close values of the fs splitting constants and were attributed to the defect center formed between nitrogen atom and vacancy. The triplet center observed in the 6H-SiC nanostructure has larger fs constant than that observed in irradiated synthetic diamond and 6H-SiC. At the same time the hf splitting due to the interaction with ^{14}N nucleus has the same value as for the triplet center observed in the n-irradiated 6H-SiC at the temperature of 5K. Taking into account that silicon vacancy (V_{Si}) is more mobile at the temperature of 900^{0}C than the carbon (V_C) vacancy and appears to dominate as a carrier in the process of low temperature impurity diffusion into the n-type 6H-SiC bulk samples, the observed triplet center was also attributed to the N-V_{Si} related center.

IV. CONCLUSION

The new electrically- and optically-detected ESR (EDESR and ODMR) technique, which allows the studies without using an external cavity and a hf source and recorder, has been demonstrated by measuring respectively the only magnetoresistance and transmission spectra. Using this new EDESR technique, the ESR spectrometer has been suggested to be replaced by the sandwich structure that represents the ultra-narrow silicon quantum well confined by the superconductor δ-barriers. These δ-barriers appeared to be the sources of the GHz and THz emission that can be enhanced by varying the dimensions of the sandwich structure which is able to form the internal cavity. This new EDESR technique has been applied to the studies of the phosphorus, iron-, hydrogen- and erbium-related centers embedded in the ultra-narrow p-type silicon quantum well that was a basis of the sandwich structure. The hf erbium structure signal has been found, for the first time, for the erbium-related centers in silicon.

The excitonic normal-mode coupling (NMC) with the single p-type Si-QW incorporated in the 1λ silicon microcavity on the n-type Si (100) wafer has been identified at T=300 K in the studies of the transmission spectra which have revealed the ODMR of the trigonal Fe-B pairs and the single carbon-hydrogen acceptor center in the absence of the external magnetic field, the external cavity and

the hf source. It is pointed out that the resonant positive magnetoresistance data can be interpreted in terms of the interference transition within frameworks of the diffusive transport of free holes in the weak anti-localization regime due to the spin relaxation processes as the external magnetic field value goes through the defect ESR resonance field corresponding to a paramagnetic center.

The ESR and EDESR studies have been shown to the isolated silicon vacancy and N-V_{Si} defect that are formed during the preparation of the planar nanostructures under the conditions of the silicon vacancy injection from the SiO_2/n-6H-SiC interface without any previous and subsequent irradiations. This planar 6H SiC nanostructure represents the ultra-shallow quantum well of the p-type confined by the δ-barriers heavily doped with boron on the n-6H SiC surface, which are self-assembled under oxidation process and subsequent short-time diffusion of boron. The EDESR measurements of the point defects in planar 6H-SiC nanostructures have been proved within frameworks of the Hall geometry by measuring the only magnetoresistance without the external cavity as well as the hf source and recorder owing to the microcavities embedded in the QW plane and internal hf generation from the δ-barriers heavily doped with boron. The EDESR spectrum of the isolated silicon vacancy revealed both negative state (S=3/2) and the neutral $V_{Si}(h)$, $V_{Si}(k_1,k_2)$ states, (S=1). Besides, N-V_{Si} defect has been found by both the EDESR method at the temperature of 77K and the ESR (X-band) method with the high sensitive ESR spectrometer Bruker ELEXSYS E580 in the temperature interval from 5K to 40K, with demonstration of very identical spectra of the triplet center (S=1). The hyperfine (hf) lines in the ESR and EDESR spectra originating from the HF interaction with the ^{14}N nucleus seem to attribute this triplet center to the N-V_{Si} defect.

The N-V_{Si} spectrum characterized by the splitting value equal to ΔB = 237.6 mT has been observed using the ESR (X-band) technique however with the nitrogen ESR spectrum corresponding to the nitrogen concentration in the n-type 6H SiC bulk crystal, $5 \cdot 10^{18}$ cm^{-3}, whereas the EDESR spectrum revealed no nitrogen centers, because of the full occupation by silicon vacancies inside the planar 6H-SiC nanostructure.

Finally, the striking result obtained in this work is that in distinction from the known N-V_{Si} defects observed in the e-irradiated diamond and in the heavy n-irradiated and high temperature annealed n-type 6H-SiC, the N-V_{Si} center characterized by the larger value of the zero-field splitting constant *D* and anisotropic *g* factor was found in the non-irradiated 6H-SiC nanostructure.

ACKNOWLEDGMENT

Authors acknowledge the support of Ioffe Institute, Russian Academy of Sciences.

REFERENCES

[1] N. T. Bagraev, W. Gehlhoff, L. E. Klyachkin, A. M. Malyarenko, V. A. Mashkov, V. V. Romanov, and T. N. Shelykh, “ODMR of impurity centers embedded in silicon microcavities,” Physica E, vol. 40, no. 5, pp. 1627-1629, March 2008.

[2] N. T. Bagraev, W. Gehlhoff, L. E. Klyachkin, A. A. Kudryavtsev, A. M. Malyarenko, G. A. Oganesyan, D. S. Poloskin, and V. V. Romanov, “Spin-dependent transport of holes in silicon quantum wells confined by superconductor barriers,” Physica C, vol. 468, no. 7-10, pp. 840-843, April 2008.

[3] N. T. Bagraev, N. G. Galkin, W. Gehlhoff, L. E. Klyachkin, and A. M. Malyarenko, “Phase and amplitude response of the ‘0.7 feature’ caused by holes in silicon one-dimensional wires and rings,” J. Phys.: Condens. Matter, vol. 20, no. 16, pp. 164202-12. April 2008.

[4] N. T. Bagraev, A. D. Bouravleuv, W. Gehlhoff, L. E. Klyachkin, A. M. Malyarenko, and V. V. Romanov, "Electron-dipole resonance of impurity centres embedded in silicon microcavities," Physica B, vol. 340-342, pp. 1078-1081, December 2003.
[5] N. T. Bagraev, A. D. Bouravleuv, W. Gehlhoff, L. E. Klyachkin, A. M. Malyarenko, and V. V. Romanov, "Electron-dipole resonance of impurity centres embedded in silicon microcavities," phys.stat.sol.(c), vol. 2, no. 2, pp. 783-786, February 2005.
[6] V. Jacques, P. Neumann, J. Beck, M. Markham, D. Twitchen, J. Meijer, F. Kaiser, G. Balasubramanian, F. Jelezko, and J. Wrachtrup, "Dynamic Polarization of Single Nuclear Spins by Optical Pumping of Nitrogen-Vacancy Color Centers in Diamond at Room Temperature," Phys. Rev. Letters, vol. 102, no. 5, pp. 057403-4, February 2009.
[7] P. G. Baranov, A. A. Soltamova, D. O. Tolmachev, N. G. Romanov, R. A. Babunts, F. M. Shakhov, S. V. Kidalov, A. Y. Vul', G. V. Mamin, S. B. Orlinskii, and N. I. Silkin, "Enormously High Concentrations of Fluorescent Nitrogen-Vacancy Centers Fabricated by Sintering of Detonation Nanodiamonds," Small, vol. 7, no. 11, pp. 1533-1537. June 2011.
[8] D. Riedel, F. Fuchs, H. Kraus, S. Väth, A. Sperlich, V. Dyakonov, A. A. Soltamova, P. G. Baranov, V. A. Ilyin, and G. V. Astakhov, "Resonant Addressing and Manipulation of Silicon Vacancy Qubits in Silicon Carbide," Phys. Rev. Letters, vol. 109, no. 22, pp. 226402-5, November 2012.
[9] P. London, J. Scheuer, J. - M.Cai, I. Schwarz, A. Retzker, M. B. Plenio, M. Katagiri, T. Teraji, M. Koizumi, J. Isoya, R. Fischer, L. P. McGuinness, B. Naydenov, and F. Jelezko, "Detecting and Polarizing Nuclear Spins with Double Resonance on a Single Electron Spin," Phys. Rev. Letters, vol. 111, no. 6, pp. 067601-5. August 2013.
[10] H. Kraus, V. A. Soltamov, D. Riedel, S. Väth, F. Fuchs, A. Sperlich, P. G. Baranov, V. Dyakonov, and G. V. Astakhov, "Room-temperature quantum microwave emitters based on spin defects in silicon carbide," Nature Physics, vol. 10, no.2, pp. 157-162. February 2014.
[11] N. T. Bagraev, V. A. Mashkov, E. Yu. Danilovsky, W. Gehlhoff, D. S. Gets, L. E. Klyachkin, A. A. Kudryavtsev, R. V. Kuzmin, A. M. Malyarenko, and V. V. Romanov, "EDESR and ODMR of Impurity Centers in Nanostructures Inserted in Silicon Microcavities," Appl. Magn. Resonance, vol. 39, no. 1-2, pp. 113-135. October 2010.
[12] J. P. Kotthaus, and R. Ranvaud, "Cyclotron resonance of holes in surface space charge layers on Si," Phys.Rev. B, vol. 15, no. 12, pp. 5758-5761, June 1977.
[13] N. T. Bagraev, W. Gehlhoff, and L. E. Klyachkin, "Cyclotron Resonance in Heavily Doped Silicon Quantum Wells," Solid St. Phenomena, vol. 47-48, pp. 589-594, July 1995.
[14] Bao-xing Li, Pen-lin Cao, and Duam-lin Que, "Distorted icosahedral cage structure of Si_{60} clusters," Phys. Rev. B, vol. 61, no. 3, pp. 1685-1687, January 2000.
[15] N. T. Bagraev, A. D. Bouravleuv, L. E. Klyachkin, A. M. Malyarenko, W. Gehlhoff, Yu. I. Romanov, and S. A. Rykov, "Local tunneling spectroscopy of silicon nanostructures," Semiconductors, vol. 39, no. 6, pp. 716-728. June 2005.
[16] N. T. Bagraev, A. D. Bouravleuv, L. E. Klyachkin, A. M. Malyarenko, W. Gehlhoff, V. K. Ivanov, and I. A. Shelykh, "Quantized conductance in silicon quantum wires," Semiconductors, vol. 36, no. 4, pp. 439-460, April 2002.
[17] A. Slaoui, E. Fogarassy, J. C. Muller, and P. Siffert, "Study of some optical and electrical properties of heavily doped silicon layers," J. de Physique Colloq., vol. 44(C5), pp. 65-71, October 1983.
[18] N. T. Bagraev, A. D. Bouravleuv, L. E. Klyachkin, A. M. Malyarenko, and S. A. Rykov, "Self-Ordered Microcavities Embedded in Ultra-shallow Silicon p-n Junctions," Semiconductors, vol. 34, no. 6, pp. 700-711, June 2000.
[19] R. Laiho, M. M. Afanasjev, M. P. Vlasenko, and L. S. Vlasenko, "Electron Exchange Interaction in S=1 Defects Observed by Level Crossing Spin Dependent Microwave Photoconductivity in Irradiated Silicon," Phys. Rev. Lett., vol. 80, no. 7, pp, 1489-1492, February 1998.

[20] N. T. Bagraev, N. G. Galkin, W. Gehlhoff, L. E. Klyachkin, A. M. Malyarenko, and I. A. Shelykh, “Spin interference in silicon one-dimensional rings,” J. Phys.:Condens. Matter, vol. 18, no. 45, pp. L567-L573, November 2006.
[21] N. T. Bagraev, N. G. Galkin, W. Gehlhoff, L. E. Klyachkin, A. M. Malyarenko, and I. A. Shelykh, “Spin interference in silicon one-dimensional rings,” Physica E, vol. 40, no. 5, pp. 1338-1340, March 2008.
[22] N. T. Bagraev, A. D. Bouravleuv, W. Gehlhoff, L. E. Klyachkin, A. M. Malyarenko, and V. V. Romanov, “Erbium-related centres embedded in silicon microcavities,” Physica B, vol. 340-342, pp. 1074-1077, December 2003.
[23] A. S. Alexandrov, and J. Ranninger, “Bipolaronic superconductivity,” Phys. Rev. B, vol. 24, no. 3, pp. 1164-1169, August 1981.
[24] A .S. Alexandrov, and N. F. Mott, “Bipolarons,” Rep. Prog. Phys., vol. 57, no. 12, pp. 1197-1288, December 1994.
[25] V. L. Ginzburg, “On surface superconductivity,” Phys. Lett., vol. 13, no. 2, pp. 101-102, November 1964.
[26] A. I. Larkin, and Yu. N. Ovchinnikov, “Nonuniform state of superconductors,” Sov. Phys. JETP, vol. 20, no. 3, pp. 762-770, March 1965.
[27] P. Fulde, and R. A. Ferrell, “Superconductivity in a Strong Spin-Exchange Field,” Phys. Rev., vol. 135, no. 3A, pp. A550-A563, August 1964.
[28] W. A. Little, “Higher temperatures: Theoretical models,” Physica, vol. 55, pp. 50-59, October 1971.
[29] N. T. Bagraev, and V .A. Mashkov, “Tunneling Negative-U Centers and Photo-Induced Reactions in Solids,” Solid State Communications, vol. 51, no. 7, pp. 515-520, August 1984.
[30] N. T. Bagraev, and V. A. Mashkov, “A mechanism for two-electron capture at deep level defects in semiconductors,” Solid State Communications, vol. 65, no. 10, pp. 1111-1117, March 1988.
[31] M. Tinkham, “Introduction to Superconductivity,” Dover, New York, 1996.
[32] N. T. Bagraev, A. A. Gippius, L. E. Klyachkin, A. M. Malyarenko, “Low Temperature Impurity Diffusion into Large-Band-Gap Semiconductors,” Mater. Sci. Forum, vol. 258-263, pp. 1833-1838, December 1997.
[33] N. T. Bagraev, E. Yu. Danilovskii, D. S. Gets, A. K. Kaveev, L. E. Klyachkin, G. I. Kropotov, A. A. Kudryavtsev, R. V. Kuzmin, A. M. Malyarenko, V. A. Mashkov, I. A. Tsibizov, D. I. Tsypishka, and I. A. Vinerov, “Terahertz emission from silicon nanostructures heavily doped with boron,” Journal of Physics: Conference Series, vol. 486, pp. 012017-4, March 2014.
[34] J. P. Reithmaier, G. Sek, A. Loffler, C. Hofmann, S. Kuhn, S. Reitzenstein, L. V. Keldysh, V. D. Kulakovskii, T. L. Reinecke, and A. Forchel, “Strong coupling in a single quantum dot-semiconductor microcavity system,” Nature, vol. 432, pp. 197-200, November 2004.
[35] I. A. Shelykh, M. A. Kulov, N. G. Galkin, and N. T. Bagraev, “Spin-dependent transport caused by the local magnetic moments inserted in the Aharonov-Bohm rings,” J. Phys.: Condens. Matter, vol. 19, no. 24, pp. 246207-21, June 2007.
[36] M. Rosenau Da Costa, I. A. Shelykh, and N. T. Bagraev, “Fractional quantization of ballistic conductance in one-dimensional hole systems,” Phys. Rev. B, vol. 76, no. 20, pp. 201302R-6, November 2007.
[37] H. H. P. Th. Bekman, T. Gregorkiewicz, and C. A. J. Ammerlaan, “Si-NL10: Paramagnetic Acceptor State of the Silicon Thermal Donor,” Phys. Rev. Lett., vol. 61, no. 2, pp. 227-230, July 1988.
[38] W. Gehlhoff, K. Irmscher, N. T. Bagraev, L. E. Klyachkin, and A. M. Malyarenko, “Shallow Centers in Heavily Doped Silicon Quantum Wells, in Shallow Level Centres in Semiconductors,” in C.A.J. Ammerlaan, B. Pajot (Eds.), Shallow Level Centres in Semiconductors, World Scientific, Singapore, 1997, pp. 227-232.

[39] Yu. V. Gorelkinskii, and N. N. Nevinnyi, "Electron paramagnetic resonance of hydrogen in silicon," Physica B, vol. 170, no. 1-4, pp. 155-167, April 1991.
[40] C. A. J. Ammerlaan, and P. T. Huy, "Characterisation of Hydrogen and Hydrogen-Related Centres in Crystalline Silicon by Magnetic-Resonance Spectroscopy," Solid State Phenom., vol. 85-86, pp. 353-414, December 2001.
[41] J. D. Carey, R. C. Barklie, J. F. Donegan, F. Priolo, G. Franzò, and S. Coffa, "Electron paramagnetic resonance and photoluminescence study of Er-impurity complexes in Si," Phys. Rev. B, vol. 59, no. 4, pp. 2773-2782, January 1999.
[42] R. Kubo, and K. Tomita, "A General Theory of Magnetic Resonance Absorption," J. Phys. Soc. Jpn., vol. 9, no. 6, pp. 888-919, November 1954.
[43] R. Kubo, "Note on the Stochastic Theory of Resonance Absorption," J. Phys. Soc. Jpn. vol. 9, no. 6, pp. 935-944, November 1954.
[44] E. C. Lightowlers, and A. N. Safonov, "Photoluminescence Vibrational Spectroscopy of Defects Containing the Light Impurities Carbon and Oxygen in Silicon," Mat. Sci. Forum, vol. 258-263, pp. 617-622, December 1997.
[45] S. Ghatnekar-Nilsson, M. Kleverman, P. Emanuelsson, and H. G. Grimmeiss, "Identification of the iron-boron line spectrum in silicon," Semicond. Sci. Technol., vol. 8, no. 10, pp. 1857-1861, October 1993.
[46] C. Weisbuch, M. Nishioka, A. Ishikawa, and Y. Arakawa, "Observation of the coupled exciton-photon mode splitting in a semiconductor quantum microcavity," Phys. Rev. Lett., vol. 69, no. 23, pp. 3314-3317, December 1992.
[47] G. Khitrova, H. M. Gibbs, F. Jahnke, M. Kira, and S. W. Koch, "Nonlinear optics of normal-mode-coupling semiconductor microcavities," Rew. Modern. Phys., vol. 71, no. 5, pp. 1591-1639, October-December 1999.
[48] A. Mainwood, "The Trapping of Hydrogen at Carbon Defects in Silicon," Mat. Sci. Forum, vol. 258-263, pp. 253-258, December 1997.
[49] A. N. Safonov, and E. C. Lightowlers, "The M-Line (760.8 me V) Luminescence System Associated with the Carbon-Hydrogen Acceptor Centre in Silicon," Mat. Sci. Forum, vol. 258-263, pp. 259-254, December 1997.
[50] P. G. Baranov, A. P. Bundakova, A. A. Soltamova, S. B. Orlinskii, I. V. Borovykh, R. Zondervan, R. Verberk, and J. Schmidt, "Silicon vacancy in SiC as a promising quantum system for single-defect and single-photon spectroscopy," Phys. Rev.B, vol. 83, no. 12, pp. 125203-12, March 2011.
[51] C. J. Cochrane, P. M. Lenahan, and A. J. Lelis, "The effect of nitric oxide anneals on silicon vacancies at and very near the interface of 4H SiC metal oxide semiconducting field effect transistors using electrically detected magnetic resonance," Applied Physics Letters, vol. 102, no. 19, pp. 193507-4, May 2013.
[52] X. - F. He, N. B. Manson, and P. T. H. Fisk, "Paramagnetic resonance of photoexcited N-V defects in diamond. II. Hyperfine interaction with the ^{14}N nucleus," Phys. Rev B, vol. 47, no. 14, pp. 8816-8822, April 1993.
[53] M. V. Muzafarova, I. V. Ilyin, E. N. Mokhov, V. I. Sankin, and P. G. Baranov, "Identification of the Triplet State N-V Defect in Neutron Irradiated Silicon Carbide by Electron Paramagnetic Resonance," Mater. Sci. Forum, vol. 527-529, pp. 555-558, October 2006.